Multiple paths lead to salt tolerance - pre-adaptation vs dynamic responses from two closely related extremophytes

Kieu-Nga Tran, Guannan Wang, Dong-Ha Oh, John C. Larkin, Aaron P. Smith, Maheshi Dassanayake*

Department of Biological Sciences, Louisiana State University, Baton Rouge, LA 70803, USA
*Address correspondence to: maheshid@lsu.edu

Keywords: Extremophyte, *Schrenkiella parvula*, *Eutrema salsugineum*, omics, convergent response, pre-adaptation, stress-preparedness, dynamic response

Abstract

Salinity stress is an ongoing problem for global crop production. *Schrenkiella parvula* and *Eutrema salsugineum* are salt-tolerant extremophytes closely related to *Arabidopsis thaliana*. We investigated multi-omics salt stress responses of the two extremophytes in comparison to *A. thaliana*. Our results reveal that *S. parvula* limits Na accumulation while *E. salsugineum* shows high tissue tolerance to excess Na. Despite this difference, both extremophytes maintained their nutrient balance, while *A. thaliana* failed to sustain its nutrient content. The root metabolite profiles of the two extremophytes, distinct at control conditions, converged upon prolonged salt stress. This convergence was achieved by a dynamic response in *S. parvula* roots increasing its amino acids and sugars to the constitutively high basal levels observed in *E. salsugineum*. The metabolomic adjustments were strongly supported by the transcriptomic responses in the extremophytes. The predominant transcriptomic signals in all three species were associated with salt stress. However, root architecture modulation mediated by negative regulators of auxin and ABA signaling supported minimally affected root growth unique to each extremophyte during salt treatments. Overall, *E. salsugineum* exhibited more preadapted responses at the metabolome level while *S. parvula* showed predominant pre-adaptation at the transcriptome level to salt stress. Our work shows that while salt

30 tolerance in these two species shares common features, they substantially differ in pathways
31 leading to convergent adaptive traits.

32 **Introduction**

33 Plants differ greatly in their tolerance to salt stress and there is a metabolic cost for
34 adaptation to salt stress, reflected by differences in growth and yield when grown in high saline
35 soils (Santiago-Rosario et al., 2021; Flowers et al., 2015). Only ~2 % of angiosperms are adapted
36 to grow in high saline environments while the remaining 98 %, including most crop plants, are
37 highly sensitive to salt stress (Flowers and Colmer, 2008; Hajiboland et al., 2018). Previous
38 studies have largely used salt-sensitive model plants or crops to understand genetic
39 mechanisms underlying salt tolerance. Insight gained from examining the molecular processes
40 in salt tolerant extremophytes contrasted to a salt-sensitive model offers a promising prospect
41 to discover tolerance mechanisms that are absent in the salt-sensitive plants and proven to be
42 evolutionary successful against salt stress.

43 *Schrenkiella parvula* and *Eutrema salsugineum* (Brassicaceae) are two extremophyte
44 models with foundational genomic resources made available. They are also closely related to
45 *Arabidopsis thaliana* making it feasible to readily deduce orthologous relationships among the
46 three models (Dassanayake et al., 2011; Wu et al., 2012). These extremophytes, currently used
47 as leading models to investigate genetic mechanisms underlying salt stress adaptation
48 (Kazachkova et al., 2018), show salt resilient growth even at salinities reaching seawater
49 strengths (Inan et al., 2004; Orsini et al., 2010; Kazachkova et al., 2018). While *S. parvula* is
50 found near salt lakes in the Irano-Turanian region (Hajiboland et al., 2018; Tug et al., 2019), *E.*
51 *salsugineum* has a wider distribution from coastal to inland saline fields in the northern
52 temperate to sub-arctic regions including the United States, Canada, Russia, and China (Lee et
53 al., 2016). Despite multiple studies highlighting some of the metabolomic and transcriptomic
54 responses of the extremophytes to salt stress (Gong et al., 2005; Kazachkova et al., 2013; Oh et
55 al., 2014; Lee et al., 2016; Prerostova et al., 2017), molecular phenotypes determining how both
56 extremophytes have convergently achieved salt adapted growth unlike their salt stress-
57 sensitive relative, *A. thaliana* have not been explored.

58 Excess salt exerts cellular stress as osmotic, oxidative, ionic, and water-deficit stresses
59 (Pantha and Dassanayake, 2020; Zhao et al., 2020; van Zelm et al., 2020). Multiple genetic
60 mechanisms mediated by ABA as well as non-ABA dependent pathways have been shown to
61 modulate salt stress responses in *A. thaliana*, all major crops, and selected halophytes
62 (Takahashi and Shinozaki, 2019; Takahashi et al., 2020; Zhao et al., 2020). These studies
63 collectively support the view that salt stress-adapted plants will show a highly coordinated
64 response to survive salt stress that requires synergistic coordination between root and shoot
65 responses. Despite the complexity of adapting to salt stress at the whole plant level, multiple
66 angiosperm lineages have evolved this complex trait repeatedly (Flowers et al., 2010; Bennett
67 et al., 2013). Therefore, it is one of the main complex traits studied for convergent evolution in
68 plants. Even if a large body of work exist to identify many of the individual cellular, molecular,
69 or physiological responses in selected tissues that contribute to salt stress adaptations, we still
70 have a large gap in understanding how a common set of orthologs from a closely related group
71 of plants selectively modulate salt stress adaptations at a cellular level (Isayenkov and
72 Maathuis, 2019) and which pathways are synergistically used to achieve salt stress adaptation
73 facilitating stress resilient growth in extremophytes.
74 In this study, we used a combined transcriptomic, ionomic, and metabolomic
75 experimental design to investigate the coordinated cellular responses of *S. parvula*, *E.*
76 *salsugineum,* and *A. thaliana* to salt treatments in root and shoot tissues. We examined the
77 coordination of multiple genetic pathways used by the three models at different salt stress
78 intensities. We identified preadapted responses mostly at the metabolome level for *E.*
79 *salsugineum* while *S. parvula* showed more stress-preparedness at the transcriptome level.
80 Additionally, both extremophyte showed molecular phenotypes suggesting induction of
81 complementary cellular processes that used core pathways present in all plants, but with
82 modifications to those in ways that optimized balance between stress tolerance and growth.
83
84 **Results**
85 Previous studies using either *S. parvula* or *E. salsugineum* in a comparative study with *A.*
86 *thaliana* have successfully used 150 mM NaCl to elicit salt stress responses in the extremophyte

87 while avoiding induction of immediate tissue necrosis in *A. thaliana* in the short-term
88 (Kazachkova et al., 2018). We grew *S. parvula, E. salsugineum*, and *A. thaliana* hydroponically
89 for 28 days, added NaCl to the growth medium (Figure S1A). *Arabidopsis thaliana* did not show
90 severe stress symptoms until four days of exposure to salt. Therefore, in our comparative
91 system with three species, we decided to capture the short-term effects of salt at 0, 3, 24, and
92 72 hr durations with 150 mM NaCl to include timepoints that would precede the onset of stress
93 phenotypes. Additionally, 250 mM NaCl was used to further deduce salt stress responses
94 induced in the extremophytes. We used the initial three timepoints to detect immediate
95 responses of the ionome and the transcriptome to salt and used 0 hr and the latter two
96 timepoints to detect the subsequent metabolome level changes (Figure S1B).
97
98 **High tissue tolerance to Na accumulation vs limiting Na accumulation in tissues**
99 All three species accumulated salt as the duration of the treatment or the concentration
100 of NaCl increased. *Arabidopsis thaliana* accumulated Na in shoots much more than in roots but
101 did not limit Na accumulation in roots compared to *S. parvula* (Figure 1A). *Arabidopsis thaliana*
102 shoots showed a 19-fold increase of Na compared to control within 24 hr. Tissue accumulation
103 of Na was remarkably low in both roots and shoots of *S. parvula* compared to the other two
104 species. Interestingly, *E. salsugineum* allowed high Na accumulation in both roots and shoots
105 compared to *S. parvula* and at levels similar to those observed for *A. thaliana* roots under salt
106 stress (Figure 1A). This suggests that *S. parvula* limited total Na accumulation in tissues while *E.*
107 *salsugineum* showed high tissue tolerance to Na accumulation, a trend maintained for 250 mM
108 NaCl treatments in extremophytes (Figure 1A). High Na levels interfere with K and other
109 nutrient uptake in plants (Munns and Tester, 2008). We examined whether Na accumulation
110 triggered nutrient imbalance in any of the test species, by quantifying the abundance of 13
111 plant nutrients during salt stress treatments. The K level significantly dropped within 3 hr in *A.*
112 *thaliana* roots but did not change in the extremophytes regardless of the duration and intensity
113 of the Na^+ treatments (Figure 1B). In shoots, we did not observe any significant changes in K
114 levels by salt stress treatments in any of the three species. When we examined the elemental
115 profiles that include all quantified nutrients, we found that shoots exhibited minimal changes in

116 all three species in response to salt stress (Figure 1C). Intriguingly, *A. thaliana* roots showed
117 significant depletion of 6 out of 13 nutrients under salt treatments whereas both
118 extremophytes showed minimal nutrient disturbances (Figure 1C and Table S1). We then
119 examined nutrient compositions in the control samples (basal levels) to identify if any nutrient
120 was preferentially enriched in any of the species (Figure 1D and Table S1). Notably, Ca and Mg,
121 which are known to aid in selectivity of Non-Selective Cation Channels (NSCCs) for K over Na in
122 plants (Shabala et al., 2006), and B were found at higher basal levels in *S. parvula* roots
123 compared to other species. Similarly, Cu and Co were high in *E. salsugineum* whereas Fe, P, K,
124 and Mo were high in *A. thaliana*.
125
126 **Primary metabolite pools decreased from high basal levels in *E. salsugineum* but increased**
127 **from low basal levels in *S. parvula* upon salt treatments**
128 Salt stress requires metabolic adjustments in plants (Pantha and Dassanayake, 2020).
129 Therefore, we examined whether the extremophytes showed similar metabolic adjustment
130 strategies that were distinct from the salt-sensitive *A. thaliana* when treated with salt. We
131 quantified a total of 716 metabolites using GC-MS for each species (see Methods), of which 182
132 with known specific structures were referred to as “known metabolites'' while the remaining
133 were collectively referred to as “unknown metabolites'' in this study (Table S2). The overall
134 quantified metabolite pool in roots showed a relatively strong correlation in metabolite
135 abundance between selected pairwise comparisons resulting in two distinct trends (Figure 2A).
136 First, the highest pairwise correlation was detected between the control groups of *S. parvula*
137 and *A. thaliana* which decreased with time as the duration of salt treatment increased (Figure
138 2A, upper panel). Second, *S. parvula* and *E. salsugineum* profiles were moderately correlated at
139 control conditions, but as both species were treated with salt, the correlation became stronger
140 indicating that the majority of metabolites in the extremophytes adjusted to similar levels in
141 the roots in response to salt treatment. This trend was observed at a shorter duration of salt
142 treatment at 24 hr when the NaCl concentration was higher at 250 mM (Fig. 2A, lower panel).
143 In contrast to roots, the shoot metabolomes of *S. parvula* and *E. salsugineum* remained
144 divergent following salt treatment (Figure S2A).

145 We also found distinct patterns in the direction of salt responses among species. Under
146 salt treatments, metabolite abundances in both *A. thaliana* and *E. salsugineum* roots largely
147 decreased while *S. parvula* increased metabolite abundances (Figure 2B). This trend for *S.*
148 *parvula* was not upheld in shoots, where all three species predominantly decreased in
149 metabolite abundances (Figure S2B). We next examined if the dynamically changing
150 metabolites were categorically associated with sugars and amino acids often known for their
151 roles as organic osmolytes (Slama et al., 2015). Figure 2C shows percent abundance among the
152 three species at control levels in roots, for all sugars, amino acids, and their immediate
153 derivatives (see Methods) quantified in our study that showed significant difference at basal
154 level abundance. Even before the salt treatment, *E. salsugineum* had accumulated much higher
155 levels for most of these metabolites than the other species. For instance, the percent
156 abundance of sucrose in *E. salsugineum* accounted for 98.6 % of the combined sucrose
157 abundance in the roots of all three species (Figure 2C) and this was 155- and 131-fold higher
158 than that in *A. thaliana*, and *S. parvula*, respectively (Table S2). Similarly, glucose, raffinose, and
159 fructose sugars and proline were much higher in *E. salsugineum* compared to the other species
160 (Figures 2C and Table S2).
161 We then tested the possibility of one extremophyte maintaining a higher basal
162 abundance for key metabolites associated with osmoregulation while the other extremophyte
163 actively induced those under salt stress, eventually converging to a metabolic status distinct
164 from that of *A. thaliana* under salt stress, as we observed in Figure 2A. We clustered the
165 profiles of all 146 known metabolites that changed abundance significantly differently at basal
166 level or in at least one stress condition from roots of all three species (Figure 2D). Two readily
167 identifiable clusters emerged (boxes outlined in Figure 2D), composed of metabolites that
168 showed lower abundances in *A. thaliana* and *S. parvula* at the control condition compared to *E.*
169 *salsugineum*, but increased in abundance exclusively in *S. parvula* upon prolonged salt
170 treatment, to the high level constitutively found in *E. salsugineum*. These clusters were
171 enriched in metabolites known for their role as osmoprotectants or antioxidants (Slama et al.,
172 2015), including sucrose, fructose, glucose, GABA, proline, and dehydroascorbic acid (full list in
173 Table S3). These results indicate a basal level metabolic "preparedness" in *E. salsugineum* roots

174 compared to active induction of many osmoprotectants and antioxidants in *S. parvula* when
175 responding to salt treatments. On the other hand, *A. thaliana* lacks neither a preadapted- nor
176 dynamic-strategy found in the two extremophytes.
177
178 ***A. thaliana* showed stronger transcriptomic responses compared to the extremophytes**
179 **during salt stress**
180 Previous studies have reported that nearly 20 % of the *A. thaliana* transcriptome
181 responds to salt stress (Gong et al., 2005; Oh et al., 2014). We tested if the transcriptomic salt
182 responses from *A. thaliana* aligned more with either extremophyte or if the extremophytes
183 showed a largely overlapping response that were distinguished from *A. thaliana*. The overall
184 root and shoot transcriptome profiles were grouped into species-tissue clusters (Figures 3A,
185 S3). This dominant species-level distinctions in transcript profiles were further demonstrated
186 with pairwise correlations of entire transcriptome profiles where none of the comparisons
187 showed correlations (Figure S3) unlike the similarities detected in metabolite profiles (Figure 2A
188 and Figure S2A). Among differently regulated genes (DEGs), we observed more transcripts
189 induced, than suppressed, by salt treatments in all three species, and the majority of the DEGs
190 were identified in 1-to-1 ortholog groups (OGs) (see Methods) (Figure 3B, Table S4). *A. thaliana*
191 showed the largest number of DEGs in response to salt stress in both roots and shoots. The *A.*
192 *thaliana* shoot transcriptome contained more than twice the number of DEGs than in the root
193 transcriptome (Figure 3B), despite fewer changes in the nutrient profile were observed in the
194 shoot than in the root (Figure 1C). Notably, the shoot transcriptome of *A. thaliana* included
195 orders of magnitude more salt-responsive DEGs than those of the extremophytes.
196 We next examined if transcriptomic changes in cellular homeostasis functions during
197 salt stress observed for *A. thaliana* entailed processes already maintained or induced in the
198 extremophytes. This search was done at two levels. First, we clustered expression of all 1-to-1
199 orthologs at their basal level (from control samples), filtered the clusters to show expression
200 patterns that differed at least in one species compared to the other two, and identified
201 enriched cellular processes in each cluster (Table 1). Responses associated with abiotic stress
202 were among the top highly representative processes in each of these functional clusters.

203 Second, we investigated the changes in transcriptomic profiles during salt treatments, by
204 identifying functional clusters enriched among all OGs that included at least one DEG in a
205 species, for roots and shoots separately (Figure 3C and Table S5 and S6). Response to stress
206 formed the largest functional cluster including the most OGs in both roots and shoots (RC1 and
207 SC1 in Figure 3C), which were further sub-clustered to highlight various salt responsive
208 pathways mediated by auxin and ABA regulation and oxidative stress responses (Figure S4).
209 Interestingly, amino acid metabolism (RC2) and sugar metabolism (RC3) formed the next two
210 largest root clusters followed by transmembrane transport (RC4) and ion transport (RC5)
211 (Figure 3C). In shoots, the second and third largest functional clusters (SC2 and SC3 in Figure 3C)
212 suggested cellular processes involved in plant development and growth/cell cycle, in which the
213 majority of the *A. thaliana* orthologs were notably salt-repressed. While the *A. thaliana*
214 orthologs were the most regulated among these OGs, extremophytes responded in similar
215 functional processes associated with abiotic stresses when treated with 250 mM NaCl (Figure
216 S5).
217 We have identified ortholog clusters showing salt-responsive co-expression across time
218 points within tissues per species. We present the two most dominant co-expression clusters in
219 roots and shoots (Figure 3D and Table S7). In roots, the largest co-expression cluster showed *A.*
220 *thaliana* orthologs substantially salt-induced compared to a much smaller magnitude of
221 induction seen in the extremophyte orthologs (Figure 3D- left panel). In shoots, the largest co-
222 expression cluster included *A. thaliana* orthologs suppressed in response to salt while
223 expression of extremophyte orthologs were stable (Figure 3D- right panel).
224
225 **The predominant transcriptomic signature in roots supports divergent auxin-dependent root**
226 **growth during salt stress**
227 In all three species, response to stress was the most representative function in roots
228 enriched among ortholog sets showing either different basal-level expression (Table 1) or salt-
229 responses (Figure 3C) among species. The most dominant sub-functional clusters/processes
230 was response to hormones in all ortholog sets especially in roots (Table 1, Figure S4A, and
231 Figure S5 A and C). Hormonal regulation plays an important role in salt stress responses (Yu et

232 al., 2020). Furthermore, our comparative ortholog expression profiling suggested that
233 regulation of hormone signal transduction was distinct among the target species (Figures 4A, S6
234 and Table S8). We found that genes mediating auxin response via auxin/indole acetic acid
235 (Aux/IAA) repressors (Gallei et al., 2020) and the type 2C protein phosphatases (PP2Cs) that
236 negatively regulate abscisic acid (ABA) signaling (Hauser et al., 2011) showed contrasting salt-
237 responsive expression among the three species, while those of other regulatory phases in auxin
238 and ABA signaling together with other hormone signaling pathways largely conserved (Figures
239 4A, S6, and Table S8). Notably, none of the *AUX/IAAs* and *PP2Cs* showed any differential
240 expression in response to salt in *S. parvula* while 15 out of total 24 *AUX/IAAs* and *PP2Cs*
241 orthologs in the other two species were significantly induced when treated with salt (Figure
242 4A). When the basal expression was compared, 11 out of 17 *E. salsugineum AUX/IAAs* orthologs
243 and 5 out of 7 *S. parvula PP2Cs* orthologs showed higher levels compared to their respective
244 orthologs in the other species (Figure 4A, the bottom panel, and Table S8).
245 Auxin and ABA suppress root elongation and lateral root initiation during salt stress in *A.*
246 *thaliana* (Ding and De Smet, 2013; Ding et al., 2015). Therefore, we first curated genes involved
247 in primary root development (GO:0080022) and lateral root development (GO:0048527) and
248 checked for functionally verified phenotypes associated with them that describe root growth in
249 *A. thaliana*. Then, we assigned a binary category of promoted or suppressed root growth to the
250 orthologs based on their basal expression levels in our target species and the genetically
251 verified functions of *A. thaliana* ortholog (see a full list of references used for the selected
252 genotype-phenotype associations in Table S9). We identified 35 single-copy orthologs that
253 showed a distinct expression level in one species compared to the other two species and
254 assigned their binary category on their effects on root growth, given their presumed effect on
255 root phenotypes (Figures 4B). We further mapped them to a lateral root development gene
256 network (modified from Banda et al., 2019; De Rybel et al., 2010 and Figure S7). Among the
257 total of 35, we found 27 orthologs in *S. parvula* to suggest increased primary root elongation or
258 suppressed lateral root initiation compared to the other species, while 23 orthologs in *E.*
259 *salsugineum* suggested slower primary and lateral root growth (Figure 4B and S7).
260 Contrastingly, *A. thaliana* showed 25 orthologs that supported its fast primary root growth and

261 increased lateral root number. Notably, the majority (71%) of the 35 orthologs were annotated
262 as auxin-responsive genes (Figure 4B).
263 In line with the observed difference in expression of orthologs associated with root
264 development (Figure 4B), *S. parvula* and *A. thaliana* seedlings have comparable primary root
265 lengths at control conditions, longer than that in *E. salsugineum* (Figure 4C and D). Moreover, *S.*
266 *parvula* showed uncompromised primary root growth compared to *E. salsugineum* and *A.*
267 *thaliana* when treated with salt for an extended time (Figures 4C, D, S8). *S. parvula* and *E.*
268 *salsugineum* seedlings also had fewer lateral roots compared to *A. thaliana* at control
269 conditions (Figure 4E). However, lateral root growth, assessed using total lateral root number
270 and density during a week-long salt treatment, indicated that *S. parvula* not only sustained
271 uninterrupted root growth but also induced lateral root growth upon salt treatment, in contrast
272 to the responses observed for *A. thaliana* and *E. salsugineum* (Figure 4E, F, and S8).
273 We aimed to further identify orthologs in *S. parvula* that may support its uninterrupted
274 primary and lateral root initiation during salt stress that distinguishes it from the other two
275 species. Therefore, we checked co-expression clusters that included differentially expressed
276 ortholog groups (OGs) in roots and found two clusters where *S. parvula* showed a different
277 pattern compared to the other two species (Figure 4G). The first cluster showed salt-induced
278 expression uniquely observed for *S. parvula.* This accounted for 11% (294 ortholog groups) of
279 differentially expressed OGs (DEOGs) in roots (Table S10). The second cluster with 113 OGs (5%
280 of all root DEOGs) groups showed induction of genes in response to salt stress in *A. thaliana*
281 and *E. salsugineum* while the orthologs in *S. parvula* did not alter their expression (Figure 4G).
282 Interestingly, within these two clusters, nearly 50% of orthologs did not have a specific GO
283 annotation indicating the level of functional obscurity associated with those genes that
284 uniquely respond in *S. parvula* to salt stress (Table S10).
285
286 **Salt-responsive transcriptome-metabolome coordination supports cellular protection in**
287 **extremophytes**
288 In response to salt treatments there were a total of 7852 orthologs identified as
289 differentially expressed genes (DEGs) and a total of 634 metabolites identified as differently

290 abundant metabolites (DAMs) for the three species in all salt treatments (Figures 2 and 3, Table
291 S2 and 4). The difference in % change in response to salt between DAMs and DEGs was the
292 lowest in *A. thaliana*, while in extremophytes metabolic responses were relatively larger
293 compared to the overall transcriptomic response during salt treatments (Figure 5A and S9A).
294 This indicates that there is more transcriptome level preparedness to respond to salt in the
295 extremophytes than in *A. thaliana*.

296 The second and third largest functional clusters over-represented among DEOGs in roots
297 were amino acid and sugar metabolism (550 orthologs) in roots (Figure 3C, RC2 and RC3).
298 Additionally, our overall metabolite response indicated a high correlation of metabolite levels
299 between the two extremophytes *S. parvula* and *E. salsugineum* during salt treatments, and the
300 DAMs shared between the extremophytes were enriched in amino acids and sugars (Figure 2).
301 Collectively, these findings led us to examine whether DEGs associated with amino acid and
302 sugar metabolism support a salt-induced metabolic response associated with amino acid and
303 sugars in the extremophytes. In line with the global trend (Figure 5A), we observed fewer DEGs
304 associated with amino acid and sugar metabolism in both extremophyte roots than in *A.*
305 *thaliana* roots, but more amino acid and sugar metabolites were found as DAMs in
306 extremophytes in roots (Figure 5B).

307 Given the established role of amino acids and sugars as organic osmoprotectants during
308 salt stress (Slama et al., 2015), we focused on the most highly responsive DAMs that are also
309 osmoprotectants and the key genes that are involved in the metabolism of those metabolite
310 (Figures 5 C and D, and S9A). Proline was one of the most significant DAMs found in roots of
311 both extremophytes that not only had a higher basal level than in *A. thaliana*, but also its
312 abundance further increased with salt treatments concordantly with the transcriptional
313 induction of *pyrroline-5-carboxylate synthetase* (*P5CS1*) and suppression of *Pro-dehydrogenase*
314 (*ProDH1*) in extremophytes (Figure 5C and S9B). Furthermore, shikimic acid derived amino
315 acids, tyrosine, and phenylalanine (precursors of phenylpropanoids) showed higher basal levels
316 or significant induction in roots of both extremophytes compared to *A. thaliana* (Figure 5C).
317 Interestingly, genes coding for the enzymes directly involved in the conversion of
318 phosphoenolpyruvate to shikimic acid such as DAHPS1, DAHPS2, DHQS, DHQ, SK1, ESPS, and CS

319 were not detected as DEGs in any of the three species (Figure S9C). However, *MYB15,* a master
320 regulator of shikimic acid biosynthesis pathway (Chen et al., 2006), was highly induced in all
321 three species (Figure 5C). *Chorismate mutases 1* (*CM1*), coding for the enzyme involved in the
322 first committed step of tyrosine and phenylalanine biosynthesis was salt-induced in *E.*
323 *salsugineum*, while it was constitutively expressed at a high level in *S. parvula* (Figure 5C).
324 *E. salsugineum* maintained a higher basal abundance than the other two species for
325 multiple sugars in roots used as organic osmolytes in plants, while these metabolites increased
326 their abundances in response to salt in *S. parvula* (Figure 5D). The genes involved in the
327 biosynthesis of these metabolites such as *sucrose synthase 1* (*SUS1*), *cell wall invertase 1*
328 (*cwIN1*), *galactinol synthase 2* (*GolS2*), and *raffinose synthase* were mostly induced under salt
329 or constitutively expressed with high basal levels in the extremophytes (Figure 5D). This
330 concordant alignment of DAMs and DEGs or maintenance of high constitutive abundance of
331 metabolites with high basal expression of genes highlighted for osmoprotectants in the
332 extremophytes was similar to coordination observed between known antioxidants and their
333 associated genes such as the dehydroascorbic acid pathway (Figure S9D).
334
335 **Coordination between nutrient balance and gene expression associated with ion transport**
336 Two other dominant functional clusters in roots, including 156 OGs, assessed using salt
337 stress responsive ortholog groups identified ion transport and membrane transport as the main
338 processes, (Figure 3C, RC4 and RC5). We also observed extremophyte ionomic profiles that
339 maintained nutrient balance unlike that of *A. thaliana* during salt treatments (Figure 1C).
340 Hence, we investigated all 148 *A. thaliana* genes encoding transporters based on Araport 11
341 annotation (Cheng et al., 2017) in the following four categories: (1) aquaporins (*PIPs*, *NIPs*, *TIPs*,
342 and *SIPs*), (2) cation transporters (*CAXs*, *NHXs*, *KEAs*, *CHXs*, *KUPs*, *HKT1*, and *TRH1*), (3) non-
343 selective cation channels (*CNGCs* and *GLRs*), and (4) K channels (*SKOR, GORK, AKTs* and *KCOs*).
344 We found 109 corresponding one-to-one ortholog groups (OGs), among which 64 OGs were
345 differentially expressed at basal level in the three species (Table S11). We focused on the OGs
346 encoding transporters and channels that were expressed at significantly different basal levels in
347 both extremophytes compared to *A. thaliana* (Figure 6A). Genes encoding transporters known

348 to exclude Na from the cell (*SOS1*), transporters involved in Ca uptake and transport (*CNGC1*,
349 *CNGC12*, *CAX1*, and *CAX5*), K channel (*KAT1*), and endosomal K transporter (*KEA5*) that aid in
350 pH and ion homeostasis (Zhu et al., 2018; Sustr et al., 2019) showed higher basal expression in
351 the extremophytes than the *A. thaliana* orthologs, while genes involved in K efflux/Na influx to
352 the cell or water transport such as *TIP1;1*, *PIP2;2*, *SIP1;2, SIP2;1*, *KUP5/6/10/11*, and *NHX3*
353 (Figure 6A). *NHX1/2*, the main transporters involved in Na sequestration in the vacuole, showed
354 higher basal level expression in *E. salsugineum* compared to the other two species (Table S11).
355 We then examined how these transporter classes changed in expression in the three
356 species when treated with salt (Figure 6B and Table S12). Interestingly, the majority of the
357 genes across the four categories were either induced or constant in expression during salt
358 treatments in *S. parvula*, whereas *A. thaliana* and *E. salsugineum* had a mixed response (Figure
359 6B). Notably, *E. salsugineum* mostly repressed the expression of genes encoding non-selective
360 cation channels (e.g. *GLRs*) in response to all salt treatments (Figure 6B and Table S12). Other
361 observable trends included the induction of *CHX17* (functions in K uptake) identified as the only
362 induced transporter in all three species in our selected set, a 50-fold induction of *CHX2*
363 (involved in Na transport to vacuole) in A. *thaliana* (Table S12), and *GORK* as the only K channel
364 up-regulated in *E. salsugineum* under salt treatment while maintaining high basal level
365 expression in *S. parvula*.
366 We next expanded the focus on the transporter genes to include copy number variation
367 among species and expression partitioned to paralogs present in each species (Figure 6C). We
368 searched for transporter gene orthologs with increased copy numbers in the extremophytes:
369 *SpNIP6;1/2* in *S. parvula*, *EsCNGC4;1/2* in *E. salsugineum*, *SpKUP9;1/2* and *EsKUP9;1/2* in both
370 extremophytes (Figure 6C, top panels, and Table S13). All extremophyte paralogs either showed
371 differential expression in response to salt or high constitutive expression compared to *A.*
372 *thaliana* (Figure 6C, bottom panels).
373 Finally, we examined the expression profiles of all non-Na/K transporters involved in
374 nutrient uptake that were included in an ortholog group in Figure 3C functional clusters RC4
375 and RC5 (Figure 6D and Table S13). Notably, *S. parvula* induced orthologs encoding a large and
376 diverse set of transporters involved in nutrient uptake upon salt treatments, while *A. thaliana*

377 and *E. salsugineum* showed salt-induction of a limited group associated with Fe, Zn, and Cu
378 uptake (e.g. *FER1/2/3*, *MTPB1*, *ZF14*, *ZIP2/11,*) (Figure 6D).
379
380 **Discussion**
381 The direct flow of Na^+ ions into plant tissue is unavoidable in saline soils. Plants show
382 adaptations at varying degrees to limit accumulation of Na^+ or mitigate cellular toxicity caused
383 by Na^+ in tissues when exposed to increasing levels of salt (Flowers and Colmer, 2008; Pantha
384 and Dassanayake, 2020; Santiago-Rosario et al., 2021). In the tolerance spectrum for salt, *S.*
385 *parvula* and *E. salsugineum* are considered halophytes whereas *A. thaliana* is not (Kazachkova
386 et al., 2018). We show that both extremophytes accumulate less Na at the whole plant level
387 than *A. thaliana* during salt treatments, with *S. parvula* accumulating the lowest levels (Figure
388 1A), consistent with previous reports (Volkov et al., 2004; Ghars et al., 2008; Oh et al., 2014).
389 Figure 7 summarizes the most notable ionomic, metabolomic, transcriptomic, and phenotypic
390 adjustments that distinguish each model plant from the other two when responding to salt
391 treatments.
392
393 **Upholding nutrient balance is a shared outcome in the extremophytes when responding to**
394 **increasing external salt levels**
395 When compared to *A. thaliana*, which loses its nutrient balance under salt stress as the
396 Na content increases (Figure 1A-C), the two extremophytes present two distinct paths for
397 regulating Na levels in roots coincident to how each plant achieves nutrient balance as a shared
398 outcome. *S. parvula* regulates Na accumulation to maintain it at levels observed for control
399 conditions, while preventing the loss or maintaining the uptake of K and Ca during salt stress. In
400 contrast, *E. salsugineum* does not show such a restriction to Na accumulation in roots but
401 reaches the same outcome as *S. parvula* for both 150 and 250 mM NaCl treatments at 24 hr
402 preventing a significant drop in its K and Ca contents.
403 Regulation of Ca levels coordinated with K is a critical requirement for ion homeostasis
404 and excess Na in plant tissues when exposed to salt stress challenges this balance (Flowers and
405 Colmer, 2008; Pantha and Dassanayake, 2020). Ca activates the efflux of Na via SOS2-SOS3

406 signaling pathway which in turn activates the plasma membrane localized Na-exporter, *SOS1*
407 (Halfter et al., 2000). Additionally, the plasma membrane localized non-selective cation
408 channels (NSCCs) are reportedly a main entry point of Na into root cells and are regulated by Ca
409 (Demidchik and Tester, 2002; Han et al., 2014). Genes encoding for NSCCs are highly
410 suppressed in *E. salsugineum* consistent with previous findings during salt stress (Volkov and
411 Amtmann, 2006) (Figure 6B and 7). However, counterintuitively, these *NSCCs* were induced or
412 unaltered in *S. parvula* during salt treatments (Figure 6B), while *S. parvula* maintains a relatively
413 smaller Na content than *E. salsugineum* when treated with salt (Figure 1A). The high basal level
414 of Ca in *S. parvula* roots may alleviate Na-induced cellular toxicity by limiting the selectivity of
415 NSCCs to Na (Han et al., 2014) (Figure 1C). This suggests that Ca may play a key role to achieve
416 ion homeostasis in *S. parvula* during salt stress at a much higher level than reported for *A.*
417 *thaliana* (Choi et al., 2014).
418 Halophytes are known for their ability to maintain high K/Na ratios in roots when
419 exposed to salt even if the species-dependent ratios can have large differences between
420 halophytes compared to more salt-sensitive species (Flowers and Colmer, 2008; Cuin et al.,
421 2008; Sun et al., 2009; Cheng et al., 2015). Under salt stress, the negative effect of Na-induced
422 membrane depolarization at the root epidermis could be reversed by the activation of K
423 outward rectifying channel, *GORK* by releasing some of the cytosolic K as shown in *A. thaliana*
424 root hairs (Ivashikina et al., 2001; Shabala and Cuin, 2008). *GORK* expression was induced in *E.*
425 *salsugineum* when exposed to 250 mM NaCl stress and maintained at high basal level in *S.*
426 *parvula* while it was low at basal level and unaltered in *A. thaliana* roots under salt stress (Table
427 S4 and 12). Therefore, it may help to prevent the membrane from further depolarization in
428 extremophytes at high salinities. However, how the extremophytes regulate their K
429 transporters to allow K uptake and simultaneously prevent excessive leakage of K during salt
430 stress is unclear. The extremophytes provide an alternative co-regulation of Na and K
431 transporters different from *A. thaliana*. One such modified pathway in the extremophytes
432 compared to *A. thaliana* from our comparative analysis point to a possible synergistic activity
433 between *GORK* and *KAT1* (K channels) synchronized with Na exclusion mediated by *SOS1* to
434 regulate cytosolic K levels, pH, and ion homeostasis in the two extremophytes when exposed to

435 salt. Coordinated expression of *GORK* and *KAT1* is a prevalent pathway mostly reported for
436 guard cells in *A. thaliana* and *KAT1* expression is thought to be highly reduced in roots (Ache et
437 al., 2000; Philippar et al., 2004). In contrast, *KAT1* is highly expressed even at basal expression
438 levels in both extremophytes (Figure 6A). Notably, these K channels are regulated by ABA and
439 auxin and both extremophytes seem to differently regulate these two hormones in conjunction
440 with overall root growth modulation in response to salt differently compared to that in *A.*
441 *thaliana* roots (Figure 4, S7, and 7). The intracellular control of K transport appears to be
442 uniquely regulated in the extremophytes compared to *A. thaliana.* For example, *KEA5* primarily
443 expressed in the trans-Golgi network (Zhu et al., 2018; Zhang et al., 2020) is expressed at much
444 higher levels in both extremophytes than in *A. thaliana* (Figures 6A and 7). Additionally, *KUP9*
445 which has undergone tandem duplication in both extremophytes, has one paralog in each
446 extremophyte that show much higher basal expression as well as induction following salt
447 treatments, in contrast to lower constitutive expression of the *A. thaliana* ortholog (Figure 6).
448 *KUP9* in *A. thaliana* mediates auxin efflux from endoplasmic reticulum (Zhang et al., 2020). It
449 would be interesting to find out if the *KUP9* duplication in the extremophytes have led to
450 divergent regulation in auxin homeostasis. Future research exploring this aspect may lead to a
451 missing link in how root growth is modulated under salt stress in salt adapted species.
452 High tissue tolerance to Na is illustrated by high Na accumulation in *E. salsugineum*
453 roots without losing its nutrient balance during salt treatments (Figure 1). This is thought to be
454 primarily facilitated by vacuolar Na-K/H transporters, *NHX1* and *NHX2* (Bassil et al., 2011). *NHX1*
455 and *NHX2* are co-induced with *V-ATPase* and this coordinated transcription concurrent to
456 increasing salt treatments is observed as expected in *E. salsugineum*, but not in the other two
457 models (Table S11 and Figure 7). *S. parvula* may have reduced the need for vacuolar
458 sequestration of Na differently from *E. salsugineum*. If it is achieved by regulating Na entry to
459 the cell via CNGCs or aquaporins as proposed by previous studies conducted on *A. thaliana*
460 (Demidchik et al., 2002; Byrt et al., 2017), transcript level coordination alone is insufficient to
461 deduce the orthologous functions in *S. parvula* as both groups are categorically highly induced
462 under salt treatments instead of being suppressed to reduce Na entry (Figure 6B).
463

464 **Metabolic preadaptation or a dynamic response equally allow adaptation to salt stress in**
465 **extremophytes**

466 Sugars, amino acids, or their associated derivatives are used in all plants for
467 osmoregulation during salt stress (Slama et al., 2015). The most striking metabolic feature
468 among the three species in our study is the extraordinary level of sugars and amino acids in *E.*
469 *salsugineum* even in control conditions compared to the other two species of which many of
470 those metabolites can serve as osmoprotectants or antioxidants (Figure 2C and 7). The
471 metabolite profiles we observed are consistent with earlier studies that examined metabolites
472 in *E. salsugineum* (Gong et al., 2005; Kazachkova et al., 2013; MacLeod et al., 2015; Lee et al.,
473 2016; Eshel et al., 2017; Shamustakimova et al., 2017; Yin et al., 2018; Pinheiro et al., 2019).
474 Previous work had suggested that *E. salsugineum* leaves and seedlings are metabolically
475 preadapted to salt stress (Gong et al., 2005; Kazachkova et al., 2013; Lee et al., 2016). Our
476 results reinforce this view and extend these observations to roots (Figure 2C and 7).
477 Complementary to a dynamic metabolic response, *S. parvula* in comparison to the other two
478 species exhibits a higher transcriptome level preadaptation to salt stress (concordant with its
479 fewer DEGs in both roots and shoots; Figures 3B and 5A). Interestingly, during salt treatments,
480 *S. parvula* which maintained much lower levels of sugars and amino acids comparable to levels
481 seen in *A. thaliana* at control conditions, raised its metabolite pools of amino acids and sugars
482 to the high basal level present in *E. salsugineum* (Figures 2 and 7).

483 Proline is among the most studied metabolites during salt stress in *E. salsugineum* and
484 generally in extremophytes due to its role as an osmoprotectant and an antioxidant (Taji et al.,
485 2004; Kant et al., 2008; Flowers and Colmer, 2008; Bartels and Dinakar, 2013). While the key
486 proline biosynthesis gene, *P5CS1* was induced in all three species under salt treatments, *Pro-*
487 *dehydrogenase* (*ProDH1*), encoding an enzyme that degrades proline, was suppressed only in
488 the extremophytes, coincident to a significant boost in proline exclusively in the extremophytes
489 (Figure 5C). The expression of *ProDH1* is known to be suppressed by sucrose (Funck et al.,
490 2010). Our results may suggest a novel regulatory alteration involving high sucrose levels
491 concomitant to the induction of *sucrose synthase* (*SUS1*) to maintain high proline levels in the
492 extremophytes via sucrose mediated suppression of *ProDH1* (Figure 5D). *A. thaliana SUS1* is

493 known to be regulated by osmotic stress independent of ABA and is also less expressed in roots
494 compared to other *SUS* members (Déjardin et al., 1999; Bieniawska et al., 2007).
495 An alternative view to why sugars and amino acids are maintained in *E. salsugineum* at
496 high levels as a preadapted feature to abiotic stress tolerance is proposed based on those
497 metabolites serving as a carbon or nitrogen source to facilitate growth when photosynthesis
498 and nitrogen acquisition may decrease with abiotic stress (Grime and Hunt, 1975; Pinheiro et
499 al., 2019; Yu et al., 2020). *E. salsugineum* roots grow much slower than both *A. thaliana* and *S.*
500 *parvula* primary roots under control conditions (Figure S8) (Orsini et al., 2010). A high
501 proportional allocation in roots for sugars such as sucrose and raffinose together with amino
502 acids known for nitrogen storage, especially proline is a common trait associated with slow
503 growing plants (Poorter, 1989; Atkinson et al., 2012). This idea aligns better with *E. salsugineum*
504 viewed as a slow growing annual compared to the other two models. Some of these
505 metabolites that are high at basal levels then have the added benefits for serving as
506 osmoprotectants or antioxidants when the plants experience high salinity levels.
507 Accumulation of sugars is reported as a metabolic trait in response to drought in *A.*
508 *thaliana* leaves (Sperdouli and Moustakas, 2012). Contradictory to viewing the accumulation of
509 sugars as a growth promoting adaptation or an adaptation to stress tolerance, it has been
510 proposed as an outcome of photosynthates passively accumulating in the absence of active
511 growth under stressed conditions (Martínez-Vilalta et al., 2016; Granda and Camarero, 2017).
512 *Schrenkiella parvula* dynamically accumulates these metabolites during salt treatments without
513 an indication of compromised growth to match the levels maintained in *E. salsugineum* (Figures
514 4 and 5 and Tran et al., 2021). The source of increased sugars in *S. parvula* is expected to result
515 from starch hydrolysis mediated by ABA upon salt stress (Thalmann et al., 2016). Therefore, at
516 least in the extremophytes, the shared outcome of high sugars and amino acids seems to be an
517 active metabolic state that could be considered as an adaptive feature to cope with salt stress
518 more than a passive outcome of excess photosynthesis under interrupted growth during stress.
519
520 **Root transcriptional networks contain multiple divergent points between the extremophytes**
521 **with convergent outcomes for stress-resilient growth**

522 *Schrenkiella parvula* and *Eutrema salsugineum* have lower lateral root densities
523 compared to *A. thaliana* (Figure 4F). Auxin is among the main hormones that regulate root
524 architecture including lateral root development (Wang et al., 2009). Lateral root initiation is
525 regulated by binding of auxin to its receptor TIR1, resulting in degradation of auxin signaling
526 repressors, the Aux/IAAs (Lakehal et al., 2019). The *TIR* orthologs in both extremophytes are
527 suppressed in control conditions coincident to successive suppression of multiple *Aux/IAAs* and
528 other downstream transcription factors in control or salt treated conditions, a pattern
529 collectively suggesting limited lateral root initiation (Banda et al., 2019) compared to *A.*
530 *thaliana* (Figure 4B and S7). Both extremophytes either having a slower root growth rate (in *E.*
531 *salsugineum*) or higher primary root growth rate but with lower lateral root density (in *S.*
532 *parvula*), which may reduce the total surface contact area with salt by reducing lateral root
533 density. Therefore, the transcriptional network mediated by auxin and other hormones in the
534 extremophytes suggests multiple regulatory points for root growth modulation that could
535 result in different root architecture (Figure S7). The overall transcriptional response promoting
536 root growth is unique to each extremophyte, but supports uninterrupted nutrient acquisition,
537 water transport, and Na^+ sequestration to synchronize both developmental and metabolic
538 coordination during salt stress differently from *A. thaliana* (Figure 4 and 6).
539 Molecular phenotypes for transcriptional preadaptation associated with multiple abiotic
540 stresses have been reported for *S. parvula* and *E. salsugineum* separately to highlight genes
541 uniformly expressed before and after stress treatments compared to differential expression of
542 orthologs in a stress sensitive sister species (Gong et al., 2005; Oh et al., 2014; Lee et al., 2016;
543 Simopoulos et al., 2020; Wang et al., 2021; Pantha et al., 2021). Our work indicated that stress-
544 associated functional gene clusters that exhibit transcriptional preadaptation in one
545 extremophyte is in many instances contrasted by a dynamic induced response by the orthologs
546 from the other extremophyte that ultimately match the expression level found in the
547 preadapted species (e.g. Figure 4G). This highlights the diversity of independent and divergent
548 regulation of orthologs even between closely related extremophytes in response to the same
549 treatments given in the same growth conditions but demonstrating different adaptive
550 strategies.

551 Overall, our study highlights the multiple different combinatorial expression modules
552 that can be examined for stress optimized growth using two extremophytes adapted to grow in
553 high salinities. The hormone-mediated root growth and especially the selective release of
554 repression in auxin and ABA signaling pathways that may lead to different *S. parvula* and *E.*
555 *salsugineum* root growth strategies absent in *A. thaliana* needs to be further investigated to
556 identify additional regulatory dependencies using target studies in the extremophyte models.
557 Similarly, comparisons from multiple extremophytes can serve as training data to identify
558 compatible regulatory pathways that can coexist but are currently absent in crops. Such
559 pathways need to be investigated for their functionality to metabolic cost to evaluate whether
560 constitutive expression (as pre-adaptive traits) or induced expression (as dynamic responses)
561 offer an optimum strategy depending on a stress condition being constant or intermittent in
562 certain environments. The scarcity of halophytes despite their recurrent evolution implies a
563 high metabolic cost and complex regulation required for salt stress adaptation for coordinated
564 growth from cellular to whole plant level (Flowers and Colmer, 2015). Extremophytes will be a
565 direct resource when modeling stress resilient growth based on which combination of core
566 stress-response pathways are critical to deliver growth and survival during environmental stress
567 (Zandalinas et al., 2021). For sustainable global food security, our crops need to be diversified,
568 less dependent on fresh water and high nutrient soils while being adapted to varying levels of
569 marginal soils with different salinities (Bailey-Serres et al., 2019; Pareek et al., 2020). Therefore,
570 basic research examining genetic regulation underlying stress optimized growth will be a
571 prerequisite when selecting new crops in light of a climate crisis.
572
573 **Materials and methods**
574 **Plant growth and treatments**
575 *Schrenkiella parvula* (ecotype Lake Tuz, Turkey; Arabidopsis Biological Resource
576 Center/ABRC germplasm CS22663)*, Eutrema salsugineum* (ecotype Shandong, China; ABRC
577 germplasm CS22504)*,* and *Arabidopsis thaliana* (ecotype Col-0) seeds were surface-sterilized
578 and stratified at 4 °C for 7 days (for *A. thaliana* and *S. parvula*) or 14 days (for *E. salsugineum*).
579 Stratified seeds were germinated and grown in a hydroponic system as described by Conn et al.,

580 (2013) for transcriptomic, ionomic, and metabolomic experiments (Figure S1B). The plants were
581 grown in aerated 1/5x strength Hoagland's solution in a growth cabinet set to 22-23 °C,
582 photosynthetic photon flux density at 80-120 mM $m^{-2}s^{-1}$, and a 12 hr light / 12 hr dark cycle.
583 Fresh Hoagland's solution was replaced every two weeks. Four-week-old plants were randomly
584 placed in 1/5x strength Hoagland's solution with and without NaCl and incubated for indicated
585 duration in each experiment.
586
587 **Root growth analysis**
588 Five-day old seedlings were transferred to 1/4x MS plates supplied with 150 mM NaCl.
589 Root growth was recorded every two days for one week. Control and treated plates were
590 scanned and analyzed using ImageJ (Schneider et al., 2012) to quantify primary root length and
591 number of lateral roots. Three biological replicates were used with 7 seedlings per replicate
592 from each species.
593
594 **Elemental analysis**
595 Elemental quantification was conducted for Na, K, Ca, P, S, Mg, Fe, B, Zn, Mn, Mo, Cu,
596 Ni, and Co using Inductively Coupled Plasma - Mass Spectrometry (ICP-MS, Elan 6000 DRC-
597 PerkinElmer SCIEX) at the US Department of Agricultural Research Service at Donald Danforth
598 Plant Science Center. We used dried root and shoot samples from 3-4 biological replicates from
599 each control and treated condition harvested at 3, and 24 hr (Figure S1) processed as described
600 in Baxter et al., (2014). Changes in element contents were calculated as the $\log_2$ fold change of
601 the element level in treated samples over that in control samples and visualized with the
602 pheatmap package in R. Significant differences between treatments within species were
603 determined by one-way ANOVA followed by Tukey post-hoc test using agricolae package in R
604 with an adjusted *p*-value cutoff of 0.05. Basal level of each element per species was calculated
605 as a % contribution from each species that added to 100% for each element, using the following
606 formula: Xi/ (Ati+Spi+Esi)*100 where *Xi* represents the abundance of element *i* in *A. thaliana*, *S.*
607 *parvula* and *E. salsugineum*, respectively. Only elements that showed significant differences in
608 abundance among the three species were visualized on ternary diagrams using ggtern R.

609

610 **Metabolite analysis**

611 Untargeted high throughput metabolite profiling was conducted using gas
612 chromatography-mass spectrometry (GC-MS) service at the West Coast Metabolomics Center,
613 University of California Davis. Root and shoot samples in 4 biological replicates were harvested
614 at 24, and 72 hr (Figure S1B), flash frozen in liquid N_2, and processed as described in Fiehn
615 (2017) and quantified as described in Pantha et al., (2021).

616 Pearson correlation coefficients per each test condition were calculated between
617 species using normalized metabolite abundances. Significant differences in metabolite
618 abundances across treatments within species (differently abundant metabolites, DAMs) was
619 determined by one-way ANOVA followed by Tukey post-hoc test using an agricolae package in R
620 with an adjusted *p*-value cutoff of 0.05. Structurally annotated (known) metabolites were
621 further categorized into functional groups according to the refmet database
622 (https://www.metabolomicsworkbench.org/databases/refmet/index.php) and Kyoto
623 Encyclopedia of Genes and Genomes (KEGG). Metabolites were clustered into amino acids,
624 sugars, nucleic acids, and other organic acids. Derivatives or precursors of those were included
625 in the same metabolite category if those individual metabolites were found to be within three
626 steps of the main metabolite category identified in a KEGG pathway (Table S2). Basal level of
627 each metabolite per species was calculated as a % contribution from each species that added to
628 100% for each metabolite similar to the elemental basal level calculation described earlier.
629 Metabolites that showed significant differences in abundance at basal level or under salt
630 treatments at least in one species were used for K-mean clustering (k= 9) (Mannor et al., 2011).
631 The metabolite profiles across samples were done using hierarchical clustering function in
632 pheatmap package.

633

634 **Orthologous group identification**

635 Ortholog groups were identified using *S. parvula* gene models version 2.2
636 (https://phytozome-next.jgi.doe.gov/); *A. thaliana* gene models version 10 (TAIR10)
637 (https://www.arabidopsis.org/download/), and *E. salsugineum* gene models (Wu et al., 2012)

638 which were updated based on reference-guided transcripte assembly using hisat2 (version
639 2.0.1)-stringtie (version 1.2.1) pipeline (Pertea et al., 2015, 2016) and RNA-seq reads from this
640 study. The updated gene models for *Eutrema salsugineum* and *Schrenkiella parvula* are
641 available at www.lsugenomics.org. The ortholog gene pairs between species were identified by
642 reciprocal blastp with default parameters and an e-value cutoff of 1E-5. The blastp results were
643 filtered using a custom python script to select the best High-scoring Segment Pair (HSPs) to
644 ensure only unique query-subject pairs were retained. Pairs with an alignment coverage smaller
645 than 50% of the query or the subject were removed. The ortholog-pair list included only non-
646 redundant pairs with the highest bit score optimized for highest % coverage, and % identity.
647 Ortholog pairs were additionally filtered to exclude any orthologs that had a more than ± 30 %
648 length difference in the coding sequence between the two sequences. A total of 16,591 one-to-
649 one ortholog groups were identified among the three species and used for all downstream
650 analyses (Table S3).
651
652 **Gene expression profiling and analysis**
653 Total RNA was extracted from control and treated samples at 3 and 24 hr with three
654 biological replicates (Figure S1) using Qiagen RNeasy Plant Mini kit, with an on-column DNase
655 treatment. mRNA enriched samples were converted to libraries using True-Seq stranded
656 RNAseq Sample Prep kit (Illumina, San Diego, CA, USA),multiplexed, and sequenced on a
657 HiSeq4000 (Illumina) platform at the Roy K. Carver Biotechnology Center, University of Illinois
658 at Urbana-Champaign. A minimum of >15 million 50-nucleotide single-end reads per sample
659 were sequenced for a total of 138 RNAseq samples.
660 After quality checks, the reads were mapped to reference transcript model sequences of
661 gene models in each species (described earlier) using Bowtie (Langmead and Slazberg, 2013)
662 with -m 1 --best -n 1 -l 50. A custom python script was used to count uniquely mapped reads for
663 each gene model. Differentially expressed genes (DEGs) across treatments within each species
664 were identified using DESeq2 (Love et al., 2014). Genes with an adjusted p-value ≤ 0.01 were
665 further filtered using the following criteria: 1) $|\log_2$ fold change$| \geq 1$ or 2) $|\log_2$ fold change$| \geq$
666 0.5 if normalized mean expression across samples ≥ 100. Genes that passed these filters were

667 considered as DEGs. Reads per kilobase per million reads (RPKM) were calculated for each gene
668 from the raw read counts for all samples. These RPKM values were log_2-transformed and
669 median-normalized when used in PCA-UMAP (McInnes et al., 2018) and for co-expression
670 cluster determinations. Co-expression clusters were done using fuzzy K-mean clustering with a
671 membership cutoff ≥ 0.4 and log2 fold change clustering. Log_2 fold changes were computed for
672 all ortholog groups (OGs) from three species, used to calculate Pearson correlation coefficients
673 when comparing transcriptome profiles between species/samples, and were visualized with
674 ggplot2 in R. Ortholog groups where at least one of the genes in the group was identified as a
675 DEG in any species under any stress condition was considered to be a differentially expressed
676 ortholog group (DEOG).
677 To compare the basal expression levels of orthologs among species, we generated a raw
678 count matrix based on reads uniquely mapped to coding sequences (CDS) for the 16,591
679 orthologs from control samples. Orthologs that are differently expressed between any two of
680 the three species were identified using DESeq2 at an adjusted *p*-value ≤ 0.001 in a pairwise
681 manner. We next assigned the expression of each gene within any given OG as High (H),
682 Medium (M), and Low (L) based on their relative expression level resulting in 12 clusters. The
683 six largest clusters in both roots and shoots highlighted the expression difference in one species
684 compared to the other two species. OGs were assigned to these clusters represented by HLH,
685 LHL, HHL, LLH, LHH, and HLL (expression profiles). Each expression profile was then subjected to
686 functional gene enrichment analysis.
687 BiNGO (Maere et al., 2005) was used to identify Gene Ontology (GO) terms enriched in
688 selected DEGs and DEOGs from shoots and roots. To reduce the redundancy between enriched
689 GO terms, we further grouped these GO terms into GO clusters using GOMCL (Wang et al.,
690 2020) with settings for -Ct 0.5 -I 1.5 -Sig 0.05 -hm -nw -hgt -d -gosize 3500 -gotype BP. Sub-
691 clustering of selected clusters was performed using GOMCL-sub with the same parameters.
692 OrthNets for selected genes were generated using the CLfinder-OrthNet pipeline with the
693 reciprocal blastp results as input using default OrthNet settings (Oh and Dassanayake, 2019),
694 and visualized in Cytoscape.
695

696 **Curated gene sets for primary metabolism, hormone signaling, root development, and**
697 **transporter functions**
698 DEOGs and OGs that showed significant differences at basal level/control condition or
699 under treatments were mapped to the KEGG pathways associated with primary metabolism,
700 hormone regulation, or root development. Log_2 fold changes were computed for all selected
701 OGs and visualized with pheatmap in R. Genes involved in root development were identified
702 from Gene Ontology annotations, GO:0048527 for lateral root development and GO:0080022
703 for primary root development. Genes coding for transport functions associated with K/Na
704 transport were mined from Araport 11. To assess the correlation between changes at the
705 transcriptomic level and the metabolic level, we calculated the percentage of DEGs and
706 differently abundant metabolites (DAMs) in each species at early (3 hr for transcriptome and 24
707 hr for metabolome) and late (24 hr for transcriptome and 72 hr for metabolome) response to
708 salt. Percent DEGs was calculated by dividing the number of DEGs by the total number of
709 expressed genes (RPKM ≥ 1) in each species. Similarly, the percent DAMs was calculated by
710 dividing the number of DAMs by the total number of quantified metabolites within a species.
711 We extracted DEGs and DAMs related to amino acid and sugar metabolism based on GO
712 (GO:0006520 for amino acid metabolism and GO:0005975 for carbohydrate metabolism). The
713 count of DEGs and DAMs were separately normalized to the total number of genes and
714 metabolites in each of the two categories.
715
716 **Data availability**
717 All Illumina sequence data are deposited at National Center for Biotechnology Information
718 BioProject PRJNA63667. Mapped RNAseq data can be browsed using genome browsers created
719 for *Schrenkiella parvula* and *Eutrema salsugineum* at www.lsugenomics.org.
720
721 **Acknowledgement**
722 This work was supported by the US National Science Foundation IOS-EDGE
723 1923589/2019610, NSF-MCB-1616827, US Department of Energy BER-DE-SC0020358, Next-
724 Generation BioGreen21 Program of Republic of Korea (PJ01317301) awards. Graduate students
725 K.T., G.W. were supported by an Economic Development Assistantship from LSU. We thank the

726 LSU High Performance Computing facility for providing computational resources;
727 undergraduate students Jordan Vivien, Christine Tran, Ashley Doan, and Jason Garcia at LSU for
728 assisting with plant growth and phenotyping; Drs. Alvaro Hernandez and John Cheeseman at
729 University of Illinois for providing assistance with Illumina sequencing.
730
731 **Author contribution**: K.T. prepared plant samples and conducted data analyses; K.T., G.W., D-
732 H.O., J.L., A.S., and M.D. contributed to data interpretation. K.T. and M.D. wrote the manuscript
733 with input from all co-authors who revised and approved the final manuscript. M.D.
734 conceptualized and supervised the overall project.
735
736 **Main figure captions**
737 **Figure 1:** Sodium accumulation and its effect on nutrient balance in the extremophytes
738 compared to *A. thaliana*. [A] Na^+ and [B] K^+ content in roots and shoots. Data are mean ± SD (n ≥
739 4, at least 4 plants per replicate). Asterisks indicate significant differences ($p \leq 0.05$) between
740 the treated samples and their respective control samples, determined by Student's t-test. Open
741 circles indicate the biological replicates. [C] Macro- and micro-nutrient fold changes between
742 treated and its respective control sample. [D] Percent abundance of nutrients that were
743 significantly different at basal levels among the three species. The three axes of the ternary
744 plots are marked with *A. thaliana, S. parvula*, and *E. salsugineum*. The gridlines in species
745 designated colors point to the relevant % abundance of the element in each axis. Significant
746 difference in elemental abundance was determined by one-way ANOVA with post-hoc Tukey's
747 test at $p \leq 0.05$.
748 **Figure 2:** Overall metabolic preparedness and adjustments in the roots of the extremophytes
749 compared to *A. thaliana*. [A] Pairwise correlation of 716 quantified metabolites(182 known, and
750 534 unknown) across all conditions and species. Correlation calculated using Pearson
751 correlation coefficients. [B] Total number of metabolites that significantly changed in
752 abundance in each species compared to its respective control sample. Known metabolite
753 numbers given in parenthesis. [C] Basal level metabolite abundances in all three species for
754 sugars, amino acids, and their derivatives. [D] Hierarchical clustering of known metabolites

755 shown in [C]. Blue box indicates clusters of interest. Treatment concentrations are 150 and 250
756 mM NaCl; Treatment durations are 24 and 72 hr. Significant differences were determined by
757 one-way ANOVA with post-hoc Tukey's test at $p \leq 0.05$ (n = 4, at least 4 plants per replicate).
758 **Figure 3:** Transcriptomic overview *S. parvula, E. salsugineum,* and *A. thaliana* in response to
759 salt. [A] Overall transcriptome clustering using one-to-one ortholog groups (OGs) in shoots and
760 roots from all replicates in all conditions. [B] Number of differently expressed genes (DEGs) in
761 response to salt treatments. [C] Functionally enriched processes clustered among OGs that
762 included a DEG from at least one species in roots and shoots. Functional annotations were
763 based on GO annotations assigned to OGs. The bar graphs assigned to each cluster represent
764 percent allocation of induced and suppressed DEGs with the number of genes that did not
765 significantly change in each species given in the white space between induced (red) and
766 suppressed (blue) bars. [D] Dominant gene expression clusters of orthologs across time points
767 and species from roots and shoots that included an *A. thaliana* ortholog that was either
768 induced or suppressed in response to salt. Differentially expressed genes identified at *p*-adj ≤
769 0.01. N= 3 (at least 4 plants per replicate).
770 **Figure 4:** Root growth responses in line with gene expression mediated by auxin and ABA in
771 *Arabidopsis thaliana, Schrenkiella parvula,* and *Eutrema salsugineum* when treated with salt.
772 [A] Expression responses of auxin/indole acetic acid (Aux/IAA) repressors and type 2C protein
773 phosphatases (PP2Cs) that regulate auxin and ABA signaling. [B] Curated genes from lateral root
774 development (GO:0048527) and primary root development (GO:0080022) used to infer root
775 growth phenotypes based on functional genetic studies in *A. thaliana*. Orthologs in the three
776 species are indicated as high (yellow), low (blue), and indistinguishable levels between species
777 (no-color) assigned to relative basal expression levels and their effect inferred with arrows (up –
778 promote growth and down – suppress growth). Genes associated with Auxin, ABA, and other
779 hormones were labeled in pink, gold, and black respectively. [C] Root growth assessment of 12-
780 day-old seedlings in response to 150 mM NaCl treated for 7 days. Quantification of [D] primary
781 root growth, [E] number of lateral roots, and [F] lateral root density. Data given as mean ± SD (n
782 = 3, at least 7 plants per replicate). Open circles indicate the measurements from each plant.
783 Asterisks indicate significant differences ($p \leq 0.05$) between treated samples and their

784 respective control samples, determined by one-way ANOVA with post-hoc Tukey's test. [G]
785 Gene co-expression clusters of differentially expressed orthologs that showed similar
786 expression pattern in *A. thaliana* and *E. salsugineum* roots compared to a different pattern
787 observed for *S. parvula* under salt stress.
788 **Figure 5:** Coordination between differently expressed genes and differently abundant
789 metabolites during responses to salt in *Arabidopsis thaliana, Schrenkiella parvula,* and *Eutrema*
790 *salsugineum*. [A] The difference in percent change in total differentially expressed genes (DEGs)
791 and total differently abundant metabolites (DAMs) in response to salt treatments. [B] % DEGs
792 and % DAMs involved in the metabolism of amino acids, sugars, and their immediate
793 derivatives (GO:0006520 and GO:0005975). [C and D] Selected pathways in amino acids and
794 sugar metabolism. Line graphs represent normalized Log2 relative metabolite abundance.
795 Boxplots represent normalized expression values. Center line shows median; box indicates
796 interquartile range (IQR); notch is for 1.58 × IQR/sqrt(n); whiskers show 1.5 × IQR. Asterisks
797 indicate DEGs and DAMs assigned using 3-4 biological replicates. Early (E) and late (L) responses
798 for transcripts refer to 3 and 24 hr. E and L responses for metabolites refer to 24 and 72 hr.
799 Metabolites are shown in the backbone of the pathway while genes encoding for key
800 enzymes/transcription factors are placed beside arrows. Black labels in pathway maps indicate
801 quantified metabolites and genes while grey labels indicate metabolites not quantified.
802 **Figure 6:** Basal and differential expression associated with salt and nutrient transport in
803 *Arabidopsis thaliana, Schrenkiella parvula,* and *Eutrema salsugineum*. [A] Basal level expression
804 given as fold changes between species. The dashed lines indicate 2-fold differences to highlight
805 genes either highly suppressed or highly expressed in the extremophytes in roots at control
806 conditions. [B] Aggregated expression profiles of transporters/channels associated with Na^+/K^+
807 transport activity during salt treatments. [C] Selected cation transporters that showed higher
808 gene copy number in extremophytes in ortholog groups and their expression during salt
809 treatments. Nodes of each ortholog network is assigned with species colors connected by edges
810 based on the relationship properties of the homologs. Edges show relationships for co-linear
811 reciprocal orthologs (cl-rc), co-linear unidirectional orthologs (cl-uni), transposed -unidirectional
812 duplicates (tr-uni), or tandem duplicated-unidirectional paralogs (td-uni). Asterisks indicate

813 differentially expressed genes identified at *p-adj ≤ 0.05 and ** p-adj ≤ 0.01. N= 3 (at least 4
814 plants per replicate). [D] Genes associated with nutrient transport identified in Figure 3C.
815 **Figure 7**: Summary of ionomic, metabolomic, transcriptomic, and phenotypic adjustments and
816 preadaptation trends to salt stress in *Arabidopsis thaliana*, *Schrenkiella parvula* and *Eutrema*
817 *salsugineum* roots. Top 9 metabolites that increased abundance in *S. parvula* were Fru,
818 fructose; Asn, asparagine, Raf, raffinose, DHA, dehydroascorbic acid; Pro, proline; Shkm,
819 shikimic acid; Suc, sucrose, GABA, gamma-aminobutyric acid; Gln, glutamine.
820 Orthologs in the three species are indicated as high (yellow), low (blue) assigned to relative
821 basal expression levels. Blue and red indicate the induction and suppression gene expression,
822 respectively. KEA5, K^+ efflux antiporter 5; KUP9, K^+ uptake permease 9; KAT1, K^+ channel in
823 *Arabidopsis thaliana* 1; GLRs, glutamate-like receptors; NHX1/2, Na^+/H^+ exchanger1/2; V-
824 ATPases, vacuoles-ATPases; SOS1, salt overly sensitive 1; GORK, gated outwardly-rectifying K^+
825 channel.
826
827 **Main table caption**
828 **Table 1**: Table 1: Enriched cellular processes of ortholog groups at basal expression level
829 clustered in shoots and roots of *S. parvula* (purple), *E. salsugineum*, (red) and *A. thaliana*
830 (green).
831
832 **Supplement figure and table captions**
833 **Figure S1**: Figure S1: Effect of salt stress on phenotype of Schrenkiella parvula (Sp), Eutrema
834 salsugineum (Es) and Arabidopsis thaliana (At). [A] Four-week-old hydroponic grown plants
835 were treated with indicated salt concentrations. [B] Experimental design and sample scheme.
836 There were at least 4 replicates used for ionomic and metabolomic profiling, and 3 replicates
837 for transcriptomic profiling with at least 4 plants per replicate.
838 **Figure S2**: Overall shoot metabolite responses in the extremophytes compared to *A. thaliana*.
839 [A] Pairwise correlation of 725 quantified metabolites across all conditions and species.
840 Correlation calculated using Pearson correlation coefficients. [B] Total number of metabolites
841 that significantly changed in abundance in each species compared to its respective control

842 sample. Known metabolite numbers given in parenthesis. [C] Basal level metabolite abundances
843 in all three species for sugars, amino acids, and their derivatives. Significant differences were
844 determined by one-way ANOVA with post-hoc Tukey's test at $p \leq 0.05$ (n = 4, at least 4 plants
845 per replicate).
846 **Figure S3:** Transcriptomic profiles of *S. parvula*, *E. salsugineum,* and *A. thaliana* were diverged
847 in response at basal level and under salt stress. [A] roots, [B] shoots. Correlation was calculated
848 using log2 fold change of treated over control samples from differentially expressed ortholog
849 pairs which included DEGs from at least one condition in one species using Pearson correlation
850 coefficients. *S. parvula* (purple), *E. salsugineum* (red) and *A. thaliana* (green).
851 **Figure S4:** Sub-clustering of dominant cluster - Response to stresses. Overlap and similarity
852 between sub-clusters determined using GO-MCL-sub and cumulative number of ortholog
853 groups (OGs) in [A and B] roots and [C and D] shoots sub-clusters.
854 **Figure S5:** Species dependent responses to salt treatments in *Schrenkiella parvula* and *Eutrema*
855 *salsugineum*. Differently expressed genes (DEGs) in *S. parvula* [A] root and [B] shoot and *E.*
856 *salsugineum* [C] root and [D] shoot in response to 150 and 250 mM NaCl stress at 3 and 24 hr of
857 treatment. Yellow highlighted data points in the Upset plots for each panel show DEGs that
858 were uniquely expressed at 250 mM salt treatments. Functionally enriched processes for these
859 selected DEGs are shown in the horizontal bar graphs given as insets outlined in yellow for each
860 panel. Differentially expressed genes identified at p-adj ≤ 0.01. N = 3 (at least 4 plants per
861 replicate).
862 **Figure S6:** Hormonal signaling pathways in response to salt treatment in *Arabidopsis thaliana,*
863 *Schrenkiella parvula,* and *Eutrema salsugineum*. Expression responses of genes associated with
864 hormonal signaling pathways obtained from KEGGs. Note that only genes that were
865 significantly different at either basal level condition or under salt treatments were shown.
866 Orthologs in the three species are indicated as high (yellow), low (blue), and indistinguishable
867 levels between species (no-color) assigned to relative basal expression levels.
868 **Figure S7:** Lateral root development gene network adopted from Banda et al., 2019 and Rybel
869 et al., 2010. The expression levels of orthologs were annotated as high (H), medium (M), or low
870 (L) relative to each other at basal levels in each ortholog group. Specific paths in the network in

871 which *S. parvula* and *E. salsugineum* consistently regulated to inhibit lateral root formation
872 were highlighted in ribbons across the network in species-specific colors.
873 **Figure S8:** Root growth of *E. salsugineum*, *S. parvula* and *A. thaliana* before and after salt
874 treatments. *S. parvula* (Sp) promoted primary root growth and reduced lateral root formation
875 while *E. salsugineum* (Es) showed slower primary root growth with reduced lateral root number
876 compared to *A. thaliana* (At) roots that showed severe root growth inhibition under salt stress.
877 Five-day-old seedlings were treated for 11 days on plates supplemented with 150 mM NaCl.
878 **Figure S9:** Metabolite abundance and expression of associated genes encoding the enzymes in
879 shikimic acid and ascorbic acid pathways. [A] percent change in total differentially expressed
880 genes (DEGs) and total differently abundant metabolites (DAMs) in response to salt treatments.
881 [B] pathway involved in proline metabolism. [C] pathway involved in the conversion from
882 phosphoenolpyruvate to chorismate. [D] pathway involved in ascorbic acid metabolism. Line
883 graphs represent normalized Log2 relative metabolite abundance. Boxplots represent
884 normalized expression values. Center line shows median; box indicates interquartile range
885 (IQR); notch is for 1.58 × IQR/sqrt(n); whiskers show 1.5 × IQR. Asterisks indicate DEGs
886 (Differently expressed genes) and DAMs (Differently abundant metabolites). Early (E) and late
887 (L) responses for transcripts refer to 3 and 24 hr. E and L responses for metabolites refer to 24
888 and 72 hr. Metabolites are shown in the backbone of the pathway while genes encoding for key
889 enzymes/transcription factors are placed beside arrows. Black labels in pathway maps indicate
890 quantified metabolites and genes while grey labels indicate metabolites not shown.
891

892 **References**

893 **Ache, P., Becker, D., Ivashikina, N., Dietrich, P., Roelfsema, M.R.G., and Hedrich, R.** (2000).
894 GORK, a delayed outward rectifier expressed in guard cells of Arabidopsis thaliana , is a K +
895 -selective, K + -sensing ion channel. FEBS Lett. **486**: 93–98.

896 **Atkinson, R.R.L., Burrell, M.M., Osborne, C.P., Rose, K.E., and Rees, M.** (2012). A non-targeted
897 metabolomics approach to quantifying differences in root storage between fast- and slow-

898 growing plants. New Phytol. **196**: 200–211.

899 **Bailey-Serres, J., Parker, J.E., Ainsworth, E.A., Oldroyd, G.E.D., and Schroeder, J.I.** (2019).
900 Genetic strategies for improving crop yields. Nature **575**: 109–118.

901 **Banda, J., Bellande, K., von Wangenheim, D., Goh, T., Guyomarc'h, S., Laplaze, L., and**
902 **Bennett, M.J.** (2019). Lateral Root Formation in Arabidopsis: A Well-Ordered LRexit.
903 Trends Plant Sci. **24**: 826–839.

904 **Bartels, D. and Dinakar, C.** (2013). Balancing salinity stress responses in halophytes and non-
905 halophytes: a comparison between Thellungiella and Arabidopsis thaliana. Funct. Plant
906 Biol. **40**: 819.

907 **Bassil, E., Tajima, H., Liang, Y.-C.Y.-C., Ohto, M.M. -a., Ushijima, K., Nakano, R., Esumi, T.,**
908 **Coku, A., Belmonte, M., and Blumwald, E.** (2011). The Arabidopsis Na+/H+ Antiporters
909 NHX1 and NHX2 Control Vacuolar pH and K+ Homeostasis to Regulate Growth, Flower
910 Development, and Reproduction. Plant Cell **23**: 3482–3497.

911 **Bennett, T.H., Flowers, T.J., and Bromham, L.** (2013). Repeated evolution of salt-tolerance in
912 grasses. Biol. Lett. **9**: 20130029.

913 **Bieniawska, Z., Paul Barratt, D.H., Garlick, A.P., Thole, V., Kruger, N.J., Martin, C., Zrenner, R.,**
914 **and Smith, A.M.** (2007). Analysis of the sucrose synthase gene family in Arabidopsis. Plant
915 J. **49**: 810–828.

916 **Byrt, C.S., Zhao, M., Kourghi, M., Bose, J., Henderson, S.W., Qiu, J., Gilliham, M., Schultz, C.,**
917 **Schwarz, M., Ramesh, S.A., Yool, A., and Tyerman, S.** (2017). Non-selective cation channel
918 activity of aquaporin AtPIP2;1 regulated by Ca 2+ and pH. Plant. Cell Environ. **40**: 802–815.

919 **Chen, Y., Zhang, X., Wu, W., Chen, Z., Gu, H., and Qu, L.-J.** (2006). Overexpression of the

920 Wounding-Responsive Gene AtMYB15 Activates the Shikimate Pathway in Arabidopsis. J.
921 Integr. Plant Biol. **48**: 1084–1095.
922 **Cheng, C.-Y.Y., Krishnakumar, V., Chan, A.P., Thibaud-Nissen, F., Schobel, S., and Town, C.D.**
923 (2017). Araport11: a complete reannotation of the Arabidopsis thaliana reference genome.
924 Plant J. **89**: 789–804.
925 **Cheng, D., Wu, G., and Zheng, Y.** (2015). Positive correlation between potassium uptake and
926 salt tolerance in wheat. Photosynthetica **53**: 447–454.
927 **Choi, W.-G., Toyota, M., Kim, S.-H., Hilleary, R., and Gilroy, S.** (2014). Salt stress-induced Ca2+
928 waves are associated with rapid, long-distance root-to-shoot signaling in plants. Proc. Natl.
929 Acad. Sci. **111**: 6497–6502.
930 **Conn, S.J., Hocking, B., Dayod, M., Xu, B., Athman, A., Henderson, S., Aukett, L., Conn, V.,**
931 **Shearer, M.K., Fuentes, S., Tyerman, S.D., and Gilliham, M.** (2013). Protocol: Optimising
932 hydroponic growth systems for nutritional and physiological analysis of Arabidopsis
933 thaliana and other plants. Plant Methods **9**: 1–11.
934 **Cuin, T.A., Betts, S.A., Chalmandrier, R., and Shabala, S.** (2008). A root's ability to retain K+
935 correlates with salt tolerance in wheat. J. Exp. Bot. **59**: 2697–2706.
936 **Dassanayake, M., Oh, D.-H., Haas, J.S., Hernandez, A., Hong, H., Ali, S., Yun, D.-J., Bressan,**
937 **R.A., Zhu, J.-K., Bohnert, H.J., and Cheeseman, J.M.** (2011). The genome of the
938 extremophile crucifer Thellungiella parvula. Nat. Genet. **43**: 913–918.
939 **Déjardin, A., Sokolov, L.N., and Kleczkowski, L.A.** (1999). Sugar/osmoticum levels modulate
940 differential abscisic acid-independent expression of two stress-responsive sucrose
941 synthase genes in Arabidopsis. Biochem. J. **344**: 503–509.

942 **Demidchik, V., Davenport, R.J., and Tester, M.** (2002). Nonselective cation channels in plants.
943 Annu. Rev. Plant Biol. **53**: 67–107.
944 **Demidchik, V. and Tester, M.** (2002). Sodium Fluxes through Nonselective Cation Channels in
945 the Plasma Membrane of Protoplasts from Arabidopsis Roots. Plant Physiol. **128**: 379–387.
946 **Ding, Z. and De Smet, I.** (2013). Localised ABA signalling mediates root growth plasticity. Trends
947 Plant Sci. **18**: 533–535.
948 **Ding, Z.J., Yan, J.Y., Li, C.X., Li, G.X., Wu, Y.R., and Zheng, S.J.** (2015). Transcription factor
949 WRKY46 modulates the development of Arabidopsis lateral roots in osmotic/salt stress
950 conditions via regulation of ABA signaling and auxin homeostasis. Plant J. **84**: 56–69.
951 **Eshel, G., Shaked, R., Kazachkova, Y., Khan, A., Eppel, A., Cisneros, A., Acuna, T., Gutterman,**
952 **Y., Tel-Zur, N., Rachmilevitch, S., Fait, A., and Barak, S.** (2017). Anastatica hierochuntica,
953 an Arabidopsis Desert Relative, Is Tolerant to Multiple Abiotic Stresses and Exhibits
954 Species-Specific and Common Stress Tolerance Strategies with Its Halophytic Relative,
955 Eutrema (Thellungiella) salsugineum. Front. Plant Sci. **7**: 1–18.
956 **Fiehn, O.** (2017). Metabolomics by Gas Chromatography-Mass Spectrometry: the combination
957 of targeted and untargeted profiling.
958 **Flowers, T.J. and Colmer, T.D.** (2015). Plant salt tolerance: Adaptations in halophytes. Ann. Bot.
959 **115**: 327–331.
960 **Flowers, T.J. and Colmer, T.D.** (2008). Salinity tolerance in halophytes. New Phytol. **179**: 945–
961 963.
962 **Flowers, T.J., Galal, H.K., and Bromham, L.** (2010). Evolution of halophytes: multiple origins of
963 salt tolerance in land plants. Funct. Plant Biol. **37**: 604.

964 **Flowers, T.J., Munns, R., and Colmer, T.D.** (2015). Sodium chloride toxicity and the cellular
965 basis of salt tolerance in halophytes. Ann. Bot. **115**: 419–431.
966 **Funck, D., Eckard, S., and Müller, G.** (2010). Non-redundant functions of two proline
967 dehydrogenase isoforms in Arabidopsis. BMC Plant Biol. **10**: 70.
968 **Gallei, M., Luschnig, C., and Friml, J.** (2020). Auxin signalling in growth: Schrödinger's cat out of
969 the bag. Curr. Opin. Plant Biol. **53**: 43–49.
970 **Ghars, M.A., Parre, E., Debez, A., Bordenave, M., Richard, L., Leport, L., Bouchereau, A.,**
971 **Savouré, A., and Abdelly, C.** (2008). Comparative salt tolerance analysis between
972 Arabidopsis thaliana and Thellungiella halophila, with special emphasis on K+/Na+
973 selectivity and proline accumulation. J. Plant Physiol. **165**: 588–599.
974 **Gong, Q., Li, P., Ma, S., Indu Rupassara, S., and Bohnert, H.J.** (2005). Salinity stress adaptation
975 competence in the extremophile Thellungiella halophila in comparison with its relative
976 Arabidopsis thaliana. Plant J. **44**: 826–839.
977 **Granda, E. and Camarero, J.J.** (2017). Drought reduces growth and stimulates sugar
978 accumulation: new evidence of environmentally driven non-structural carbohydrate use.
979 Tree Physiol. **37**: 997–1000.
980 **Grime, J. and Hunt, R.** (1975). Relative Growth-Rate : Its Range and Adaptive Significance in a
981 Local Flora. J. Ecol. **63**: 393–422.
982 **Hajiboland, R., Bahrami-Rad, S., Akhani, H., and Poschenrieder, C.** (2018). Salt tolerance
983 mechanisms in three Irano-Turanian Brassicaceae halophytes relatives of Arabidopsis
984 thaliana. J. Plant Res. **131**: 1029–1046.
985 **Halfter, U., Ishitani, M., and Zhu, J.-K.** (2000). The Arabidopsis SOS2 protein kinase physically

986 interacts with and is activated by the calcium-binding protein SOS3. Proc. Natl. Acad. Sci.
987 **97**: 3735–3740.
988 **Han, S., Wang, C., Wang, W., and Jiang, J.** (2014). Mitogen-activated protein kinase 6 controls
989 root growth in Arabidopsis by modulating Ca2+-based Na+ flux in root cell under salt
990 stress. J. Plant Physiol. **171**: 26–34.
991 **Hauser, F., Waadt, R., and Schroeder, J.I.** (2011). Evolution of Abscisic Acid Synthesis and
992 Signaling Mechanisms. Curr. Biol. **21**: R346–R355.
993 **Inan, G. et al.** (2004). Salt Cress. A Halophyte and Cryophyte Arabidopsis Relative Model System
994 and Its Applicability to Molecular Genetic Analyses of Growth and Development of
995 Extremophiles. Plant Physiol. **135**: 1718–1737.
996 **Isayenkov, S. V. and Maathuis, F.J.M.** (2019). Plant Salinity Stress: Many Unanswered
997 Questions Remain. Front. Plant Sci. **10**: 80.
998 **Ivashikina, N., Becker, D., Ache, P., Meyerhoff, O., Felle, H.H., and Hedrich, R.** (2001). K+
999 channel profile and electrical properties of Arabidopsis root hairs. FEBS Lett. **508**: 463–469.
1000 **Kant, S., Bi, Y.-M., Weretilnyk, E., Barak, S., and Rothstein, S.J.** (2008). The Arabidopsis
1001 Halophytic Relative Thellungiella halophila Tolerates Nitrogen-Limiting Conditions by
1002 Maintaining Growth, Nitrogen Uptake, and Assimilation. Plant Physiol. **147**: 1168–1180.
1003 **Kazachkova, Y., Batushansky, A., Cisneros, A., Tel-Zur, N., Fait, A., and Barak, S.** (2013).
1004 Growth Platform-Dependent and -Independent Phenotypic and Metabolic Responses of
1005 Arabidopsis and Its Halophytic Relative, Eutrema salsugineum, to Salt Stress. Plant Physiol.
1006 **162**: 1583–1598.
1007 **Kazachkova, Y., Eshel, G., Pantha, P., Cheeseman, J.M., Dassanayake, M., and Barak, S.** (2018).

1008 Halophytism: What Have We Learnt From Arabidopsis thaliana Relative Model Systems?
1009 Plant Physiol. **178**: 972–988.
1010 **Lakehal, A. et al.** (2019). A Molecular Framework for the Control of Adventitious Rooting by
1011 TIR1/AFB2-Aux/IAA-Dependent Auxin Signaling in Arabidopsis. Mol. Plant **12**: 1499–1514.
1012 **Langmead, B. and Slazberg, S.L.** (2013). Fast gapped-read alignmnet with Bowtie 2. Nat.
1013 Methods **9**: 357–359.
1014 **Lee, Y.P., Funk, C., Erban, A., Kopka, J., Köhl, K.I., Zuther, E., and Hincha, D.K.** (2016). Salt
1015 stress responses in a geographically diverse collection of Eutrema/Thellungiella spp.
1016 accessions. Funct. Plant Biol. **43**: 590–606.
1017 **Love, M.I., Huber, W., and Anders, S.** (2014). Moderated estimation of fold change and
1018 dispersion for RNA-seq data with DESeq2. Genome Biol. **15**: 1–34.
1019 **MacLeod, M.J.R., Dedrick, J., Ashton, C., Sung, W.W.L., Champigny, M.J., and Weretilnyk, E.A.**
1020 (2015). Exposure of two Eutrema salsugineum (Thellungiella salsuginea) accessions to
1021 water deficits reveals different coping strategies in response to drought. Physiol. Plant.
1022 **155**: 267–280.
1023 **Maere, S., Heymans, K., and Kuiper, M.** (2005). BiNGO: A Cytoscape plugin to assess
1024 overrepresentation of Gene Ontology categories in Biological Networks. Bioinformatics **21**:
1025 3448–3449.
1026 **Mannor, S., Jin, X., Han, J., Jin, X., Han, J., Jin, X., Han, J., and Zhang, X.** (2011). K-Means
1027 Clustering. In Encyclopedia of Machine Learning (Springer US: Boston, MA), pp. 563–564.
1028 **Martínez-Vilalta, J., Sala, A., Asensio, D., Galiano, L., Hoch, G., Palacio, S., Piper, F.I., and**
1029 **Lloret, F.** (2016). Dynamics of non-structural carbohydrates in terrestrial plants: a global

1030 synthesis. Ecol. Monogr. **86**: 495–516.

1031 **McInnes, L., Healy, J., Saul, N., and Großberger, L.** (2018). UMAP: Uniform Manifold
1032 Approximation and Projection. J. Open Source Softw. **3**: 861.

1033 **Oh, D.-H., Hong, H., Lee, S.Y., Yun, D.-J., Bohnert, H.J., and Dassanayake, M.** (2014). Genome
1034 Structures and Transcriptomes Signify Niche Adaptation for the Multiple-Ion-Tolerant
1035 Extremophyte Schrenkiella parvula. Plant Physiol. **164**: 2123–2138.

1036 **Oh, D.H. and Dassanayake, M.** (2019). Landscape of gene transposition-duplication within the
1037 Brassicaceae family. DNA Res.

1038 **Orsini, F. et al.** (2010). A comparative study of salt tolerance parameters in 11 wild relatives of
1039 Arabidopsis thaliana. J. Exp. Bot. **61**: 3787–3798.

1040 **Pantha, P. and Dassanayake, M.** (2020). Living with Salt. Innov. **1**: 100050.

1041 **Pantha, P., Oh, D.-H., Longstreth, D., and Dassanayake, M.** (2021). Living with high potassium:
1042 an asset or a hindrance. bioRxiv: 2021.07.01.450778.

1043 **Pareek, A., Dhankher, O.P., and Foyer, C.H.** (2020). Mitigating the impact of climate change on
1044 plant productivity and ecosystem sustainability. J. Exp. Bot. **71**: 451–456.

1045 **Pertea, M., Kim, D., Pertea, G.M., Leek, J.T., and Salzberg, S.L.** (2016). Transcript-level
1046 expression analysis of RNA-seq experiments with HISAT, StringTie and Ballgown. Nat.
1047 Protoc. **11**: 1650–1667.

1048 **Pertea, M., Pertea, G.M., Antonescu, C.M., Chang, T.-C., Mendell, J.T., and Salzberg, S.L.**
1049 (2015). StringTie enables improved reconstruction of a transcriptome from RNA-seq reads.
1050 Nat. Biotechnol. **33**: 290–295.

1051 **Philippar, K., Ivashikina, N., Ache, P., Christian, M., Lüthen, H., Palme, K., and Hedrich, R.**

1052 (2004). Auxin activates KAT1 and KAT2 , two K + -channel genes expressed in seedlings of
1053 Arabidopsis thaliana. Plant J. **37**: 815–827.
1054 **Pinheiro, C., Dickinson, E., Marriott, A., Ribeiro, I.C., Pintó-Marijuan, M., António, C., Zarrouk,**
1055 **O., Chaves, M.M., Dodd, I.C., Munné-Bosch, S., Thomas-Oates, J., and Wilson, J.** (2019).
1056 Distinctive phytohormonal and metabolic profiles of Arabidopsis thaliana and Eutrema
1057 salsugineum under similar soil drying. Planta **249**: 1417–1433.
1058 **Poorter, H.** (1989). Interspecific variation in relative growth rate: on ecological causes and
1059 physiological consequences. Causes consequences Var. growth rate Product. High. plants
1060 **24**: 45–68.
1061 **Prerostova, S., Dobrev, P.I., Gaudinova, A., Hosek, P., Soudek, P., Knirsch, V., and Vankova, R.**
1062 (2017). Hormonal dynamics during salt stress responses of salt-sensitive Arabidopsis
1063 thaliana and salt-tolerant Thellungiella salsuginea. Plant Sci. **264**: 188–198.
1064 **De Rybel, B. et al.** (2010). A Novel Aux/IAA28 Signaling Cascade Activates GATA23-Dependent
1065 Specification of Lateral Root Founder Cell Identity. Curr. Biol. **20**: 1697–1706.
1066 **Santiago-Rosario, L.Y., Harms, K.E., Elderd, B.D., Hart, P.B., and Dassanayake, M.** (2021). No
1067 escape: The influence of substrate sodium on plant growth and tissue sodium responses.
1068 Ecol. Evol.
1069 **Schneider, C.A., Rasband, W.S., and Eliceiri, K.W.** (2012). NIH Image to ImageJ: 25 years of
1070 image analysis. Nat. Methods.
1071 **Shabala, S. and Cuin, T.A.** (2008). Potassium transport and plant salt tolerance. Physiol. Plant.
1072 **133**: 651–669.
1073 **Shabala, S., Demidchik, V., Shabala, L., Cuin, T.A., Smith, S.J., Miller, A.J., Davies, J.M., and**

1074 **Newman, I.A.** (2006). Extracellular Ca2+ ameliorates NaCl-induced K+ loss from
1075 Arabidopsis root and leaf cells by controlling plasma membrane K +-permeable channels.
1076 Plant Physiol. **141**: 1653–1665.
1077 **Shamustakimova, A.O., Leonova, T.G., Taranov, V.V., de Boer, A.H., and Babakov, A.V.** (2017).
1078 Cold stress increases salt tolerance of the extremophytes Eutrema salsugineum
1079 (Thellungiella salsuginea) and Eutrema (Thellungiella) botschantzevii. J. Plant Physiol. **208**:
1080 128–138.
1081 **Simopoulos, C.M.A., MacLeod, M.J.R., Irani, S., Sung, W.W.L., Champigny, M.J., Summers,**
1082 **P.S., Golding, G.B., and Weretilnyk, E.A.** (2020). Coding and long non-coding RNAs provide
1083 evidence of distinct transcriptional reprogramming for two ecotypes of the extremophile
1084 plant Eutrema salsugineum undergoing water deficit stress. BMC Genomics **21**: 396.
1085 **Slama, I., Abdelly, C., Bouchereau, A., Flowers, T., and Savouré, A.** (2015). Diversity,
1086 distribution and roles of osmoprotective compounds accumulated in halophytes under
1087 abiotic stress. Ann. Bot. **115**: 433–447.
1088 **Sperdouli, I. and Moustakas, M.** (2012). Interaction of proline, sugars, and anthocyanins during
1089 photosynthetic acclimation of Arabidopsis thaliana to drought stress. J. Plant Physiol. **169**:
1090 577–585.
1091 **Sun, J. et al.** (2009). Calcium mediates root K+/Na+ homeostasis in poplar species differing in
1092 salt tolerance. Tree Physiol. **29**: 1175–1186.
1093 **Taji, T., Seki, M., Satou, M., Sakurai, T., Kobayashi, M., Ishiyama, K., Narusaka, Y., Narusaka,**
1094 **M., Zhu, J.K., and Shinozaki, K.** (2004). Comparative genomics in salt tolerance between
1095 arabidopsis and arabidopsis-related halophyte salt cress using arabidopsis microarray.

1096 Plant Physiol. **135**: 1697–1709.

1097 **Takahashi, F. and Shinozaki, K.** (2019). Long-distance signaling in plant stress response. Curr.
1098 Opin. Plant Biol. **47**: 106–111.

1099 **Takahashi, Y., Zhang, J., Hsu, P.-K., Ceciliato, P.H.O., Zhang, L., Dubeaux, G., Munemasa, S.,**
1100 **Ge, C., Zhao, Y., Hauser, F., and Schroeder, J.I.** (2020). MAP3Kinase-dependent SnRK2-
1101 kinase activation is required for abscisic acid signal transduction and rapid osmotic stress
1102 response. Nat. Commun. **11**: 12.

1103 **Thalmann, M., Pazmino, D., Seung, D., Horrer, D., Nigro, A., Meier, T., Kölling, K., Pfeifhofer,**
1104 **H.W., Zeeman, S.C., and Santelia, D.** (2016). Regulation of leaf starch degradation by
1105 abscisic acid is important for osmotic stress tolerance in plants. Plant Cell **28**: 1860–1878.

1106 **Tran, K.-N. et al.** (2021). Balancing growth amidst salinity stress – lifestyle perspectives from
1107 the extremophyte model Schrenkiella parvula. bioRxiv: 6.

1108 **Tug, G.N., Yaprak, A.E., and Vural, M.** (2019). The Floristical, Ecological, and Syntaxonomical
1109 Characteristics of Salt Marshes and Salt Steppes in Turkey. In Sabkha Ecosystems (Springer:
1110 Cham), pp. 413–446.

1111 **Volkov, V. and Amtmann, A.** (2006). Thellungiella halophila, a salt-tolerant relative of
1112 Arabidopsis thaliana, has specific root ion-channel features supporting K+/Na+
1113 homeostasis under salinity stress. Plant J. **48**: 342–353.

1114 **Volkov, V., Wang, B., Dominy, P.J., Fricke, W., and Amtmann, A.** (2004). Thellungiella
1115 halophila, a salt-tolerant relative of Arabidopsis thaliana, possesses effective mechanisms
1116 to discriminate between potassium and sodium. Plant, Cell Environ. **27**: 1–14.

1117 **Wang, G., DiTusa, S.F., Oh, D.H., Herrmann, A.D., Mendoza-Cozatl, D.G., O'Neill, M.A., Smith,**

1118 **A.P., and Dassanayake, M.** (2021). Cross species multi-omics reveals cell wall
1119 sequestration and elevated global transcript abundance as mechanisms of boron tolerance
1120 in plants. New Phytol. **230**: 1985–2000.
1121 **Wang, G., Oh, D.H., and Dassanayake, M.** (2020). GOMCL: A toolkit to cluster, evaluate, and
1122 extract non-redundant associations of Gene Ontology-based functions. BMC
1123 Bioinformatics **21**: 1–9.
1124 **Wang, Y., Li, K., and Li, X.** (2009). Auxin redistribution modulates plastic development of root
1125 system architecture under salt stress in Arabidopsis thaliana. J. Plant Physiol. **166**: 1637–
1126 1645.
1127 **Wu, H.-J. et al.** (2012). Insights into salt tolerance from the genome of Thellungiella salsuginea.
1128 Proc. Natl. Acad. Sci. **109**: 12219–12224.
1129 **Yin, J., Gosney, M.J., Dilkes, B.P., and Mickelbart, M. V.** (2018). Dark period transcriptomic and
1130 metabolic profiling of two diverse Eutrema salsugineum accessions. Plant Direct **2**: e00032.
1131 **Yu, Z., Duan, X., Luo, L., Dai, S., Ding, Z., and Xia, G.** (2020). How Plant Hormones Mediate Salt
1132 Stress Responses. Trends Plant Sci. **25**: 1117–1130.
1133 **Zandalinas, S.I., Fritschi, F.B., and Mittler, R.** (2021). Global Warming , Climate Change , and
1134 Environmental Pollution : Recipe for a Multifactorial Stress Combination Disaster. Trends
1135 Plant Sci. **26**: 588–599.
1136 **van Zelm, E., Zhang, Y., and Testerink, C.** (2020). Salt Tolerance Mechanisms of Plants. Annu.
1137 Rev. Plant Biol. **71**: 403–433.
1138 **Zhang, M., Huang, P., Ji, Y., Wang, S., Wang, S., Li, Z., Guo, Y., Ding, Z., Wu, W., and Wang, Y.**
1139 (2020). <scp>KUP</scp> 9 maintains root meristem activity by regulating K^+ and auxin

1140 homeostasis in response to low K. EMBO Rep. **21**: e50164.

1141 **Zhao, C., Zhang, H., Song, C., Zhu, J., and Shabala, S.** (2020). Mechanisms of Plant Responses

1142 and Adaptation to Soil Salinity. Innov. **1**: 100017.

1143 **Zhu, X. et al.** (2018). K + Efflux Antiporters 4, 5, and 6 Mediate pH and K + Homeostasis in

1144 Endomembrane Compartments. Plant Physiol. **178**: 1657–1678.

1145

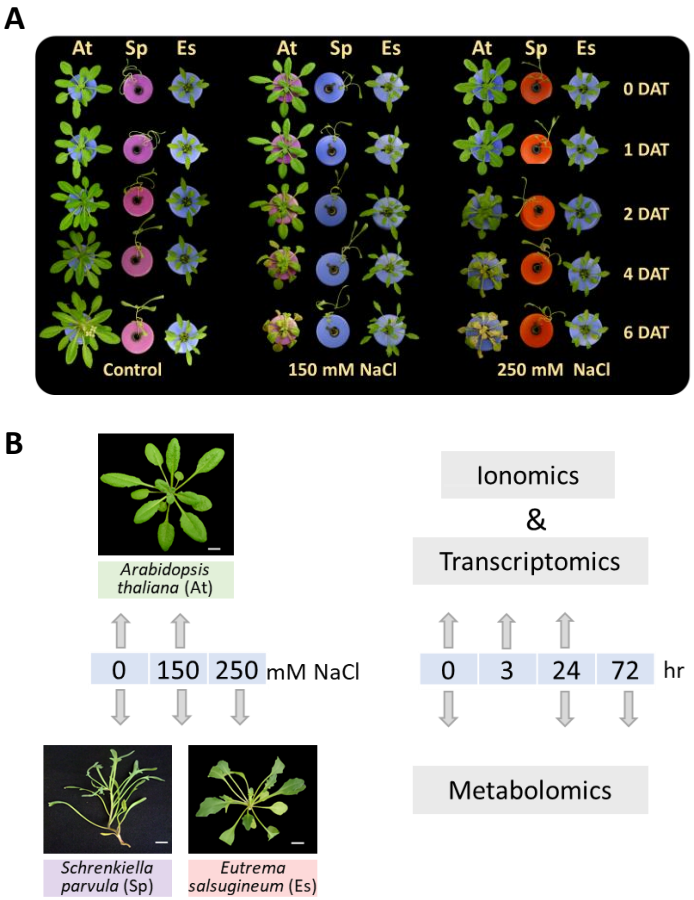

Figure S1: Effect of salt stress on phenotype of *Schrenkiella parvula* (Sp), *Eutrema salsugineum* (Es) and *Arabidopsis thaliana* (At). [A] Four-week-old hydroponic grown plants were treated with indicated salt concentrations. [B] Experimental design and sample scheme. There were at least 4 replicates used for ionomic and metabolomic profiling, and 3 replicates for transcriptomic profiling with at least 4 plants per replicate.

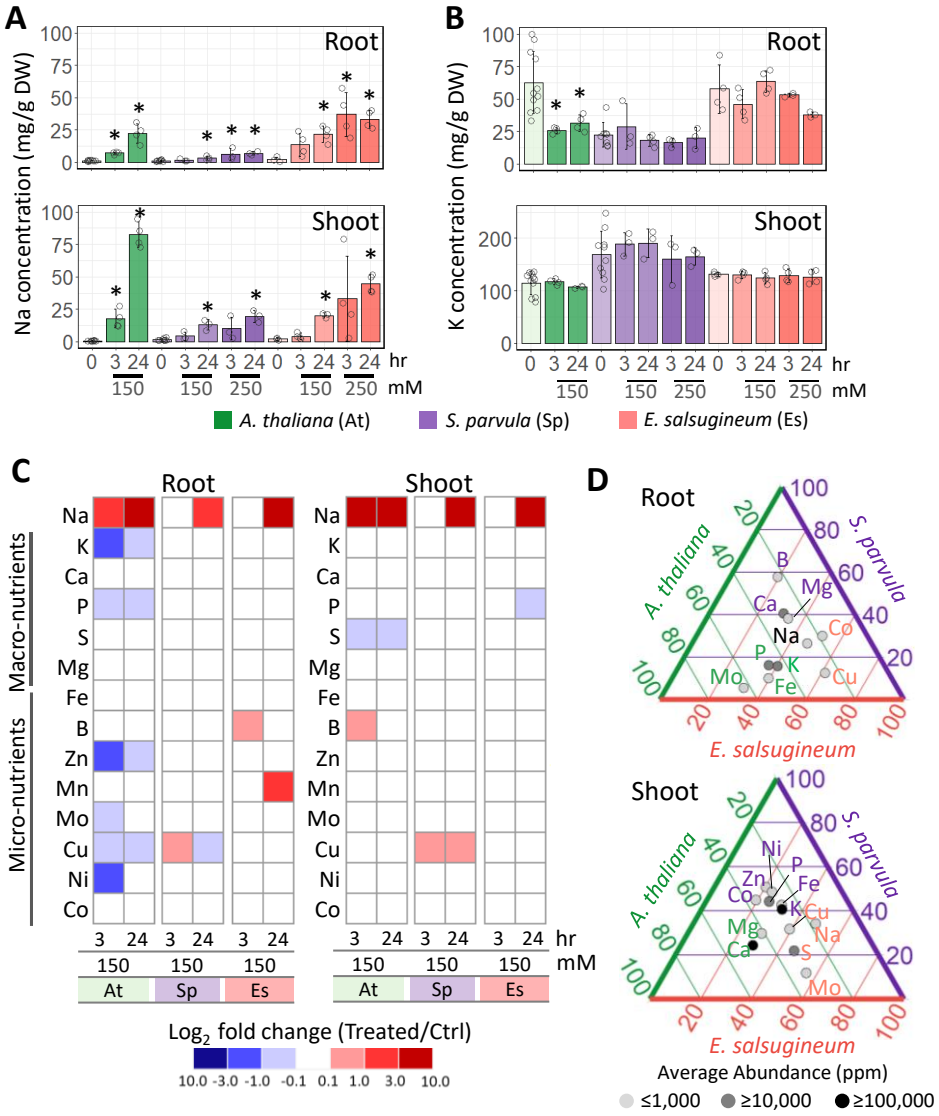

Figure 1: Sodium accumulation and its effect on nutrient balance in the extremophytes compared to *A. thaliana*. [A] Na^+ and [B] K^+ content in roots and shoots. Data are mean ± SD (n ≥ 4, at least 4 plants per replicate). Asterisks indicate significant differences ($p \leq 0.05$) between the treated samples and their respective control samples, determined by Student's t-test. Open circles indicate the biological replicates. [C] Macro- and micro-nutrient fold changes between treated and its respective control sample. [D] Percent abundance of nutrients that were significantly different at basal levels among the three species. The three axes of the ternary plots are marked with *A. thaliana, S. parvula*, and *E. salsugineum*. The gridlines in species designated colors point to the relevant % abundance of the element in each axis. Significant difference in elemental abundance was determined by one-way ANOVA with post-hoc Tukey's test at $p \leq 0.05$.

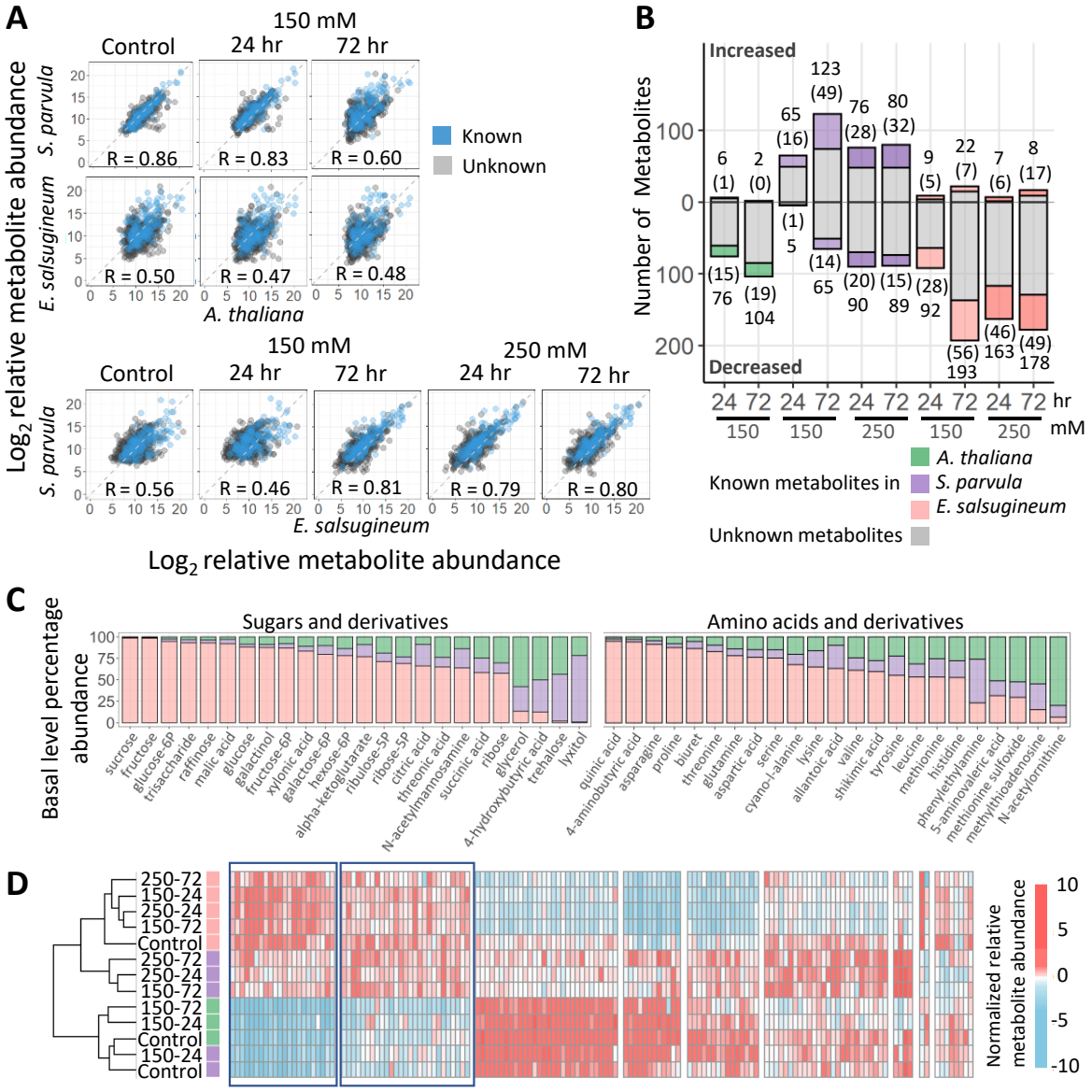

Figure 2: Overall metabolic preparedness and adjustments in the roots of the extremophytes compared to *A. thaliana*. [A] Pairwise correlation of 716 quantified metabolites (182 known, and 534 unknown) across all conditions and species. Correlation calculated using Pearson correlation coefficients. [B] Total number of metabolites that significantly changed in abundance in each species compared to its respective control sample. Known metabolite numbers given in parenthesis. [C] Basal level metabolite abundances in all three species for sugars, amino acids, and their derivatives. [D] Hierarchical clustering of known metabolites shown in [C]. Blue box indicates clusters of interest. Treatment concentrations are 150 and 250 mM NaCl; Treatment durations are 24 and 72 hr. Significant differences were determined by one-way ANOVA with post-hoc Tukey's test at $p \leq 0.05$ (n = 4, at least 4 plants per replicate).

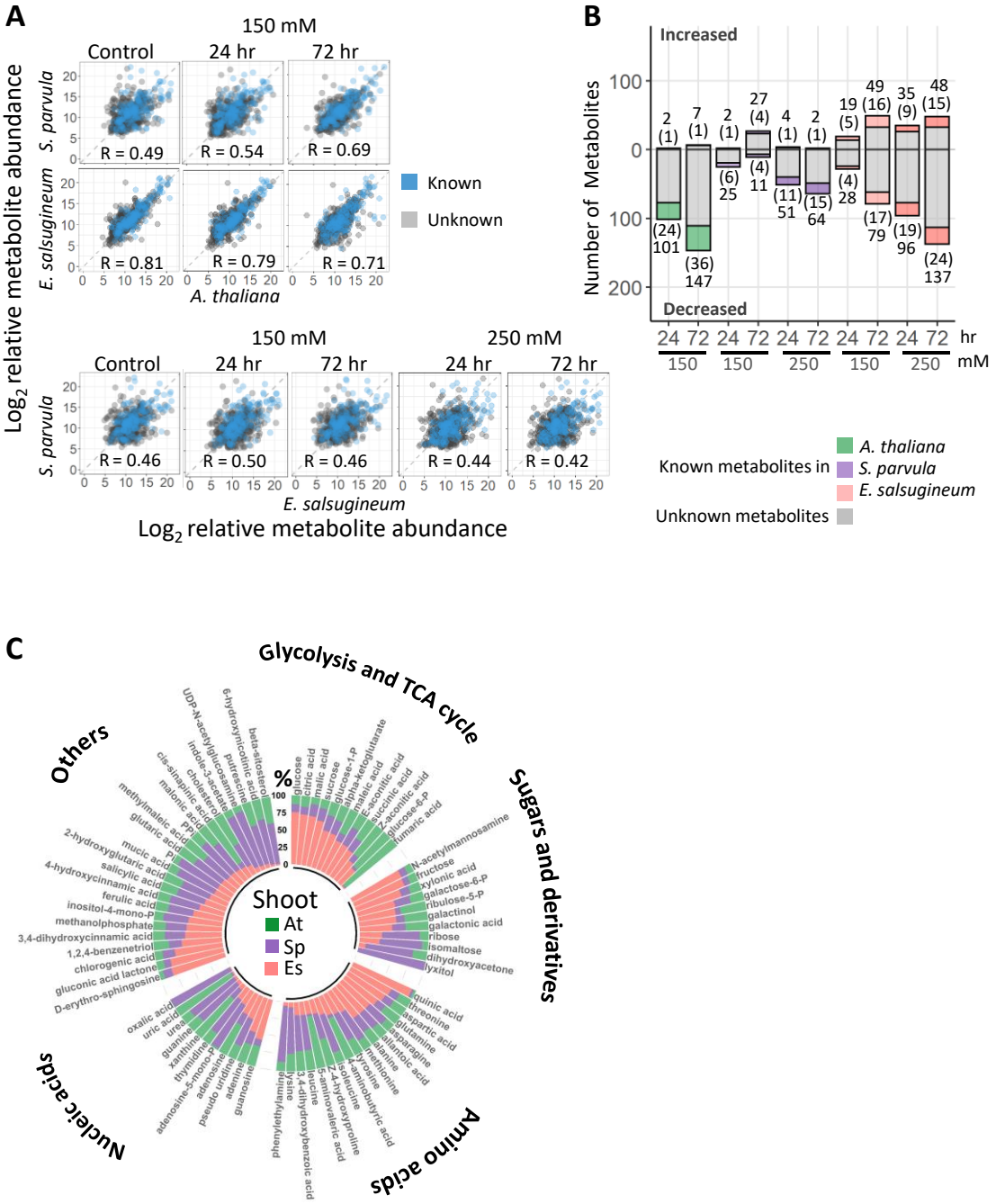

Figure S2: Overall shoot metabolite responses in the extremophytes compared to *A. thaliana*. [A] Pairwise correlation of 725 quantified metabolites across all conditions and species. Correlation calculated using Pearson correlation coefficients. [B] Total number of metabolites that significantly changed in abundance in each species compared to its respective control sample. Known metabolite numbers given in parenthesis. [C] Basal level metabolite abundances in all three species for sugars, amino acids, and their derivatives. Significant differences were determined by one-way ANOVA with post-hoc Tukey's test at $p \leq 0.05$ (n = 4, at least 4 plants per replicate).

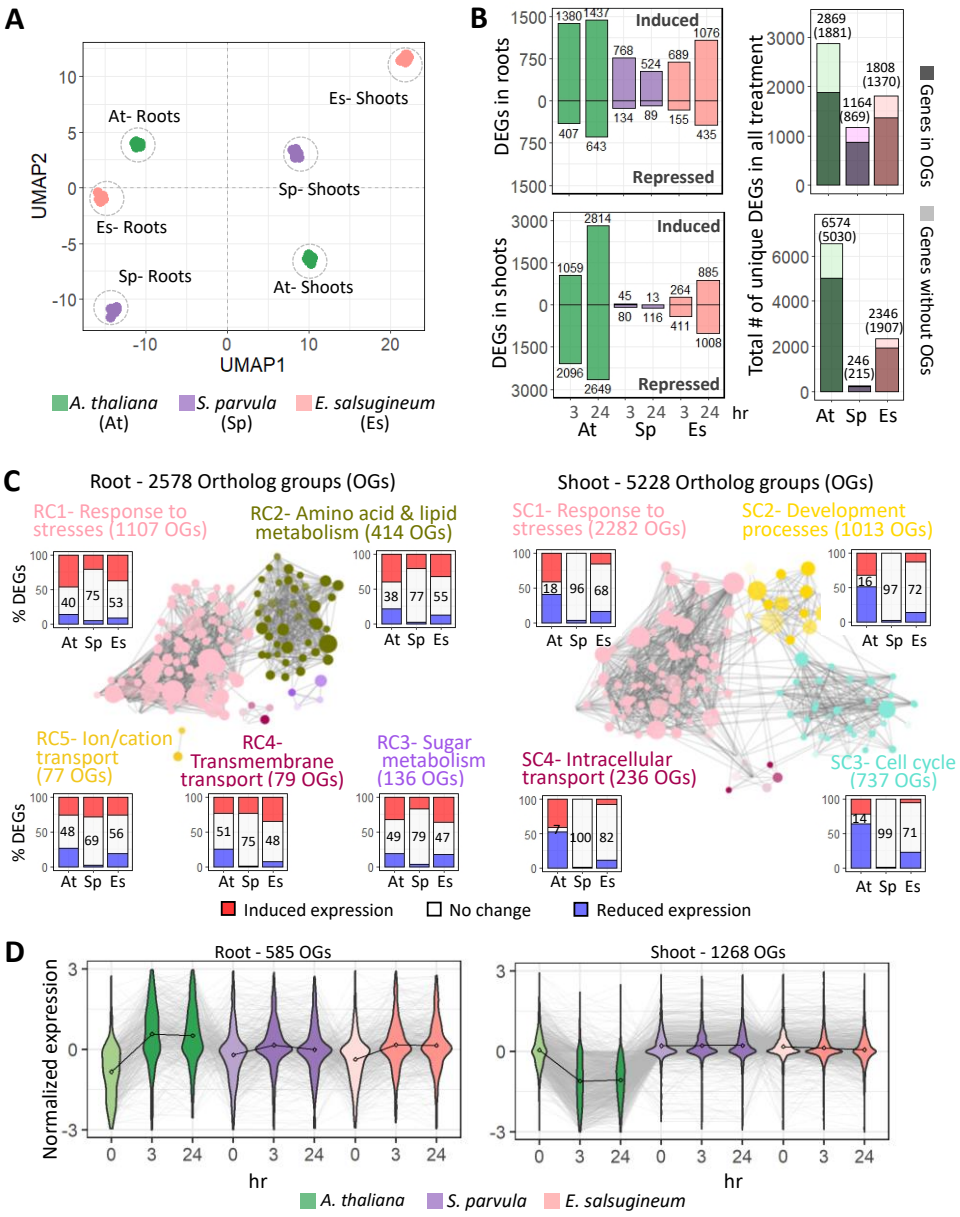

Figure 3: Transcriptomic overview *S. parvula, E. salsugineum,* and *A. thaliana* in response to salt. [A] Overall transcriptome clustering using one-to-one ortholog groups (OGs) in shoots and roots from all replicates in all conditions. [B] Number of differently expressed genes (DEGs) in response to salt treatments. [C] Functionally enriched processes clustered among OGs that included a DEG from at least one species in roots and shoots. Functional annotations were based on GO annotations assigned to OGs. The bar graphs assigned to each cluster represent percent allocation of induced and suppressed DEGs with the number of genes that did not significantly change in each species given in the white space between induced (red) and suppressed (blue) bars. [D] Dominant gene expression clusters of orthologs across time points and species from roots and shoots that included an *A. thaliana* ortholog that was either induced or suppressed in response to salt. Differentially expressed genes identified at *p*-adj ≤ 0.01. N= 3 (at least 4 plants per replicate).

Table 1: Enriched cellular processes of ortholog groups at basal expression level clustered in shoots and roots of *S. parvula* (purple), *E. salsugineum*, (red) and *A. thaliana* (green).

Patterns	Clstr	# GO	# genes	Cumulative genes %	Functional category
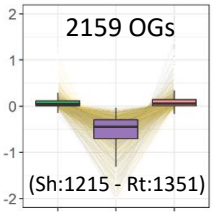	1	101	703	51.4%	Hormone and abiotic/biotic stimuli signaling
	2	58	458	70.2%	Ion and vesicular transport
	3	65	417	77.6%	Organ development
	4	26	337	82.5%	Transcriptional control of organ development
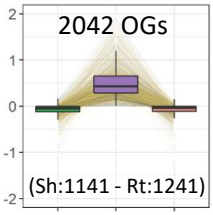	1	74	708	63.8%	Hormone and abiotic stimuli regulation
	2	83	497	88.1%	RNA and amino acid processes
	3	53	437	99.4%	Organelle biogenesis
	4	6	23	99.8%	Phospholipid metabolism
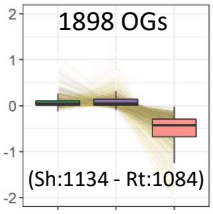	1	160	776	67.4%	Hormone and abiotic stimuli regulation
	2	100	520	88.9%	RNA and amino acid processes
	3	29	376	99%	Ion and vesicular transport
	4	4	112	99.7%	Homeostasis processes
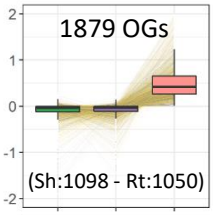	1	32	606	52.8%	Organ development
	2	58	519	74.0%	Hormone and abiotic/biotic stimuli signaling
	3	21	324	80.6%	Transcriptional regulation of development
	4	11	291	88.7%	Lipid metabolism
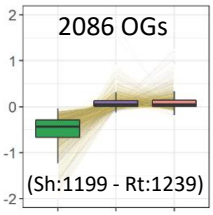	1	44	671	65.8%	RNA metabolism and gene expression
	2	11	331	82.9%	Shoot and flower development
	3	19	268	91.5%	Cell cycle regulation
	4	4	159	95.5%	Abiotic stimuli responses
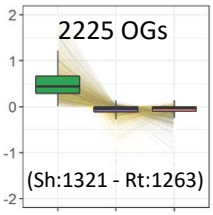	1	106	775	55.3%	Hormone and abiotic/biotic stimuli signaling
	2	92	572	72.6%	Organ development and reproduction
	3	74	398	84.4%	Amino acid & lipid metabolism
	4	43	348	92.1%	Ion and vesicular transport

Normalized expression

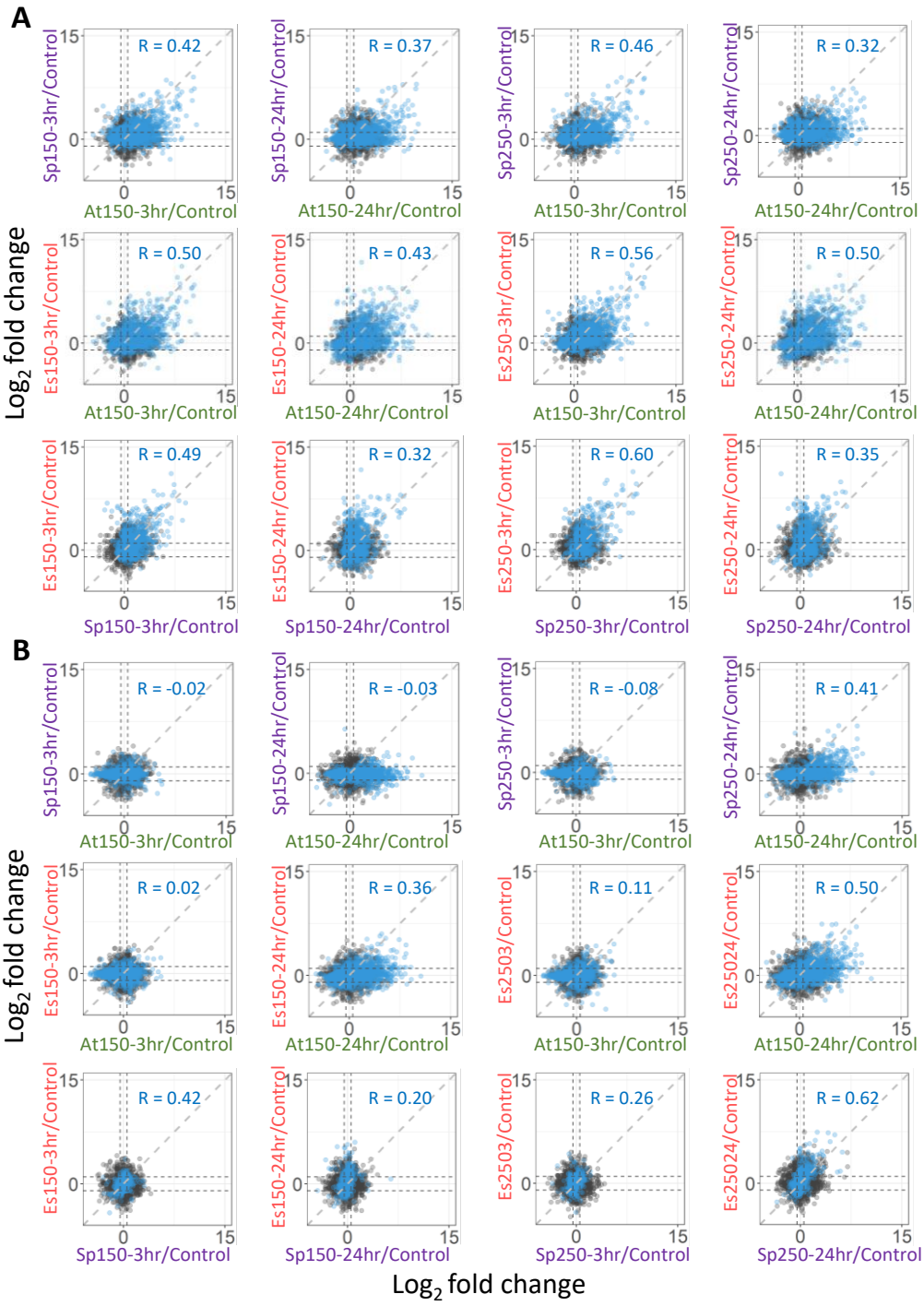

Figure S3: Transcriptomic profiles of *S. parvula*, *E. salsugineum,* and *A. thaliana* were diverged in response at basal level and under salt stress. [A] roots, [B] shoots. Correlation was calculated using log2 fold change of treated over control samples from differentially expressed ortholog pairs which included DEGs from at least one condition in one species using Pearson correlation coefficients. *S. parvula* (purple), *E. salsugineum* (red) and *A. thaliana* (green).

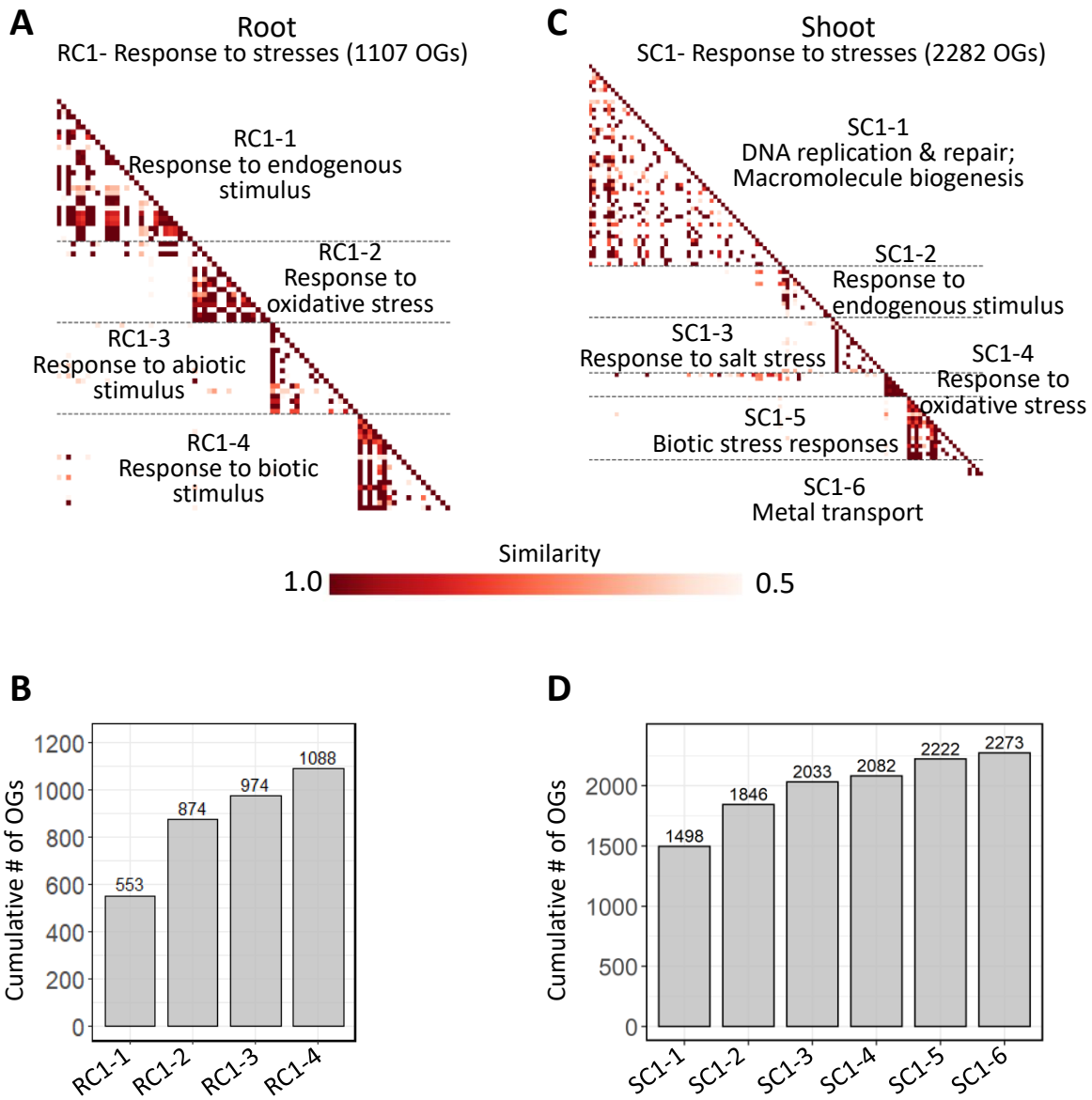

Figure S4: Sub-clustering of dominant cluster - Response to stresses. Overlap and similarity between sub-clusters determined using GO-MCL-sub and cumulative number of ortholog groups (OGs) in [A and B] roots and [C and D] shoots sub-clusters.

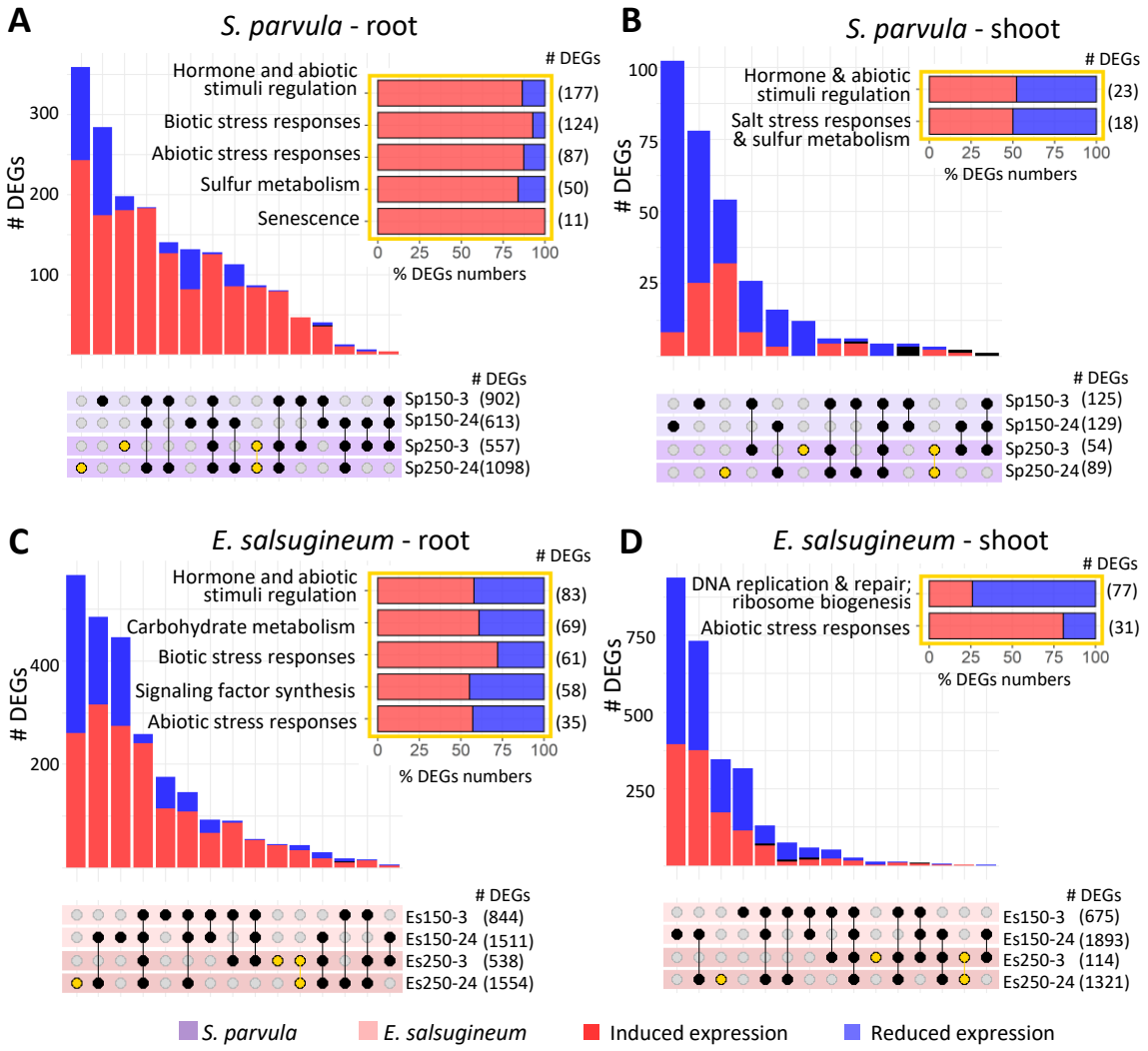

Figure S5: Species dependent responses to salt treatments in *Schrenkiella parvula* and *Eutrema salsugineum*. Differently expressed genes (DEGs) in *S. parvula* [A] root and [B] shoot and *E. salsugineum* [C] root and [D] shoot in response to 150 and 250 mM NaCl stress at 3 and 24 hr of treatment. Yellow highlighted data points in the Upset plots for each panel show DEGs that were uniquely expressed at 250 mM salt treatments. Functionally enriched processes for these selected DEGs are shown in the horizontal bar graphs given as insets outlined in yellow for each panel. Differentially expressed genes identified at *p*-adj ≤ 0.01. N = 3 (at least 4 plants per replicate).

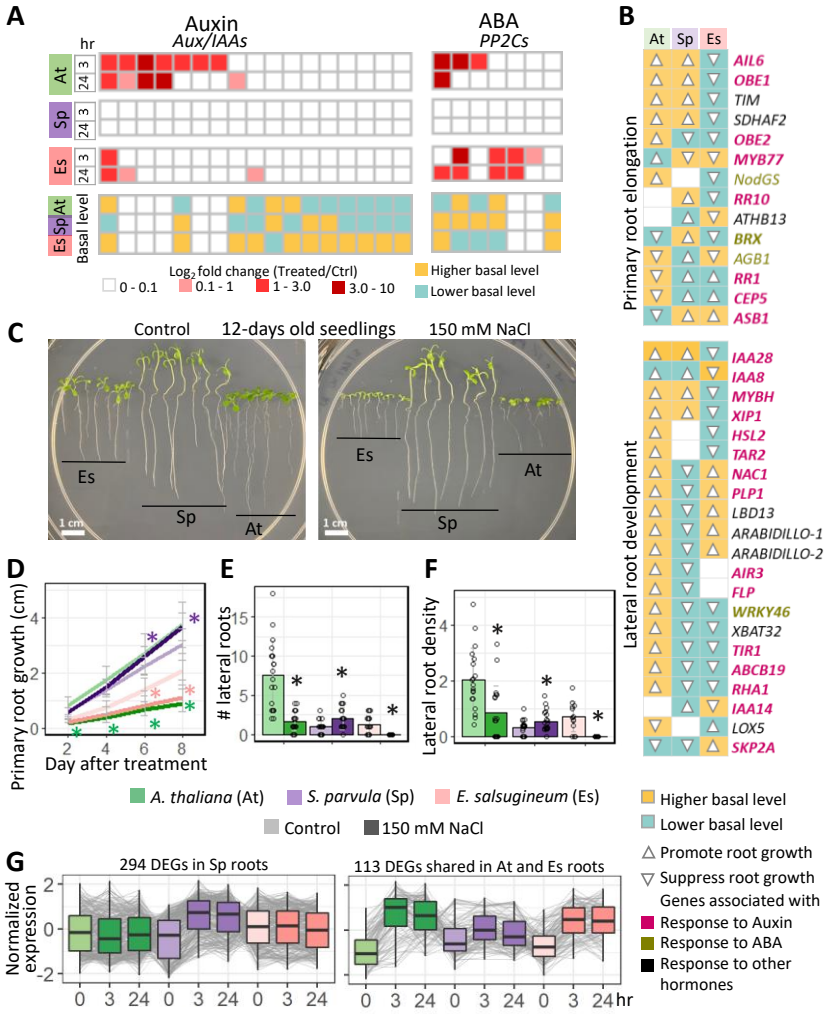

Figure 4: Root growth responses in line with gene expression mediated by auxin and ABA in *Arabidopsis thaliana, Schrenkiella parvula,* and *Eutrema salsugineum* when treated with salt. [A] Expression responses of auxin/indole acetic acid (Aux/IAA) repressors and type 2C protein phosphatases (PP2Cs) that regulate auxin and ABA signaling. [B] Curated genes from lateral root development (GO:0048527) and primary root development (GO:0080022) used to infer root growth phenotypes based on functional genetic studies in *A. thaliana*. Orthologs in the three species are indicated as high (yellow), low (blue), and indistinguishable levels between species (no-color) assigned to relative basal expression levels and their effect inferred with arrows (up – promote growth and down – suppress growth). Genes associated with Auxin, ABA, and other hormones were labeled in pink, gold, and black respectively. [C] Root growth assessment of 12-day-old seedlings in response to 150 mM NaCl treated for 7 days. Quantification of [D] primary root growth, [E] number of lateral roots, and [F] lateral root density. Data given as mean ± SD (n = 3, at least 7 plants per replicate). Open circles indicate the measurements from each plant. Asterisks indicate significant differences ($p \leq 0.05$) between treated samples and their respective control samples, determined by one-way ANOVA with post-hoc Tukey's test. [G] Gene co-expression clusters of differentially expressed orthologs that showed similar expression pattern in *A. thaliana* and *E. salsugineum* roots compared to a different pattern observed for *S. parvula* under salt stress.

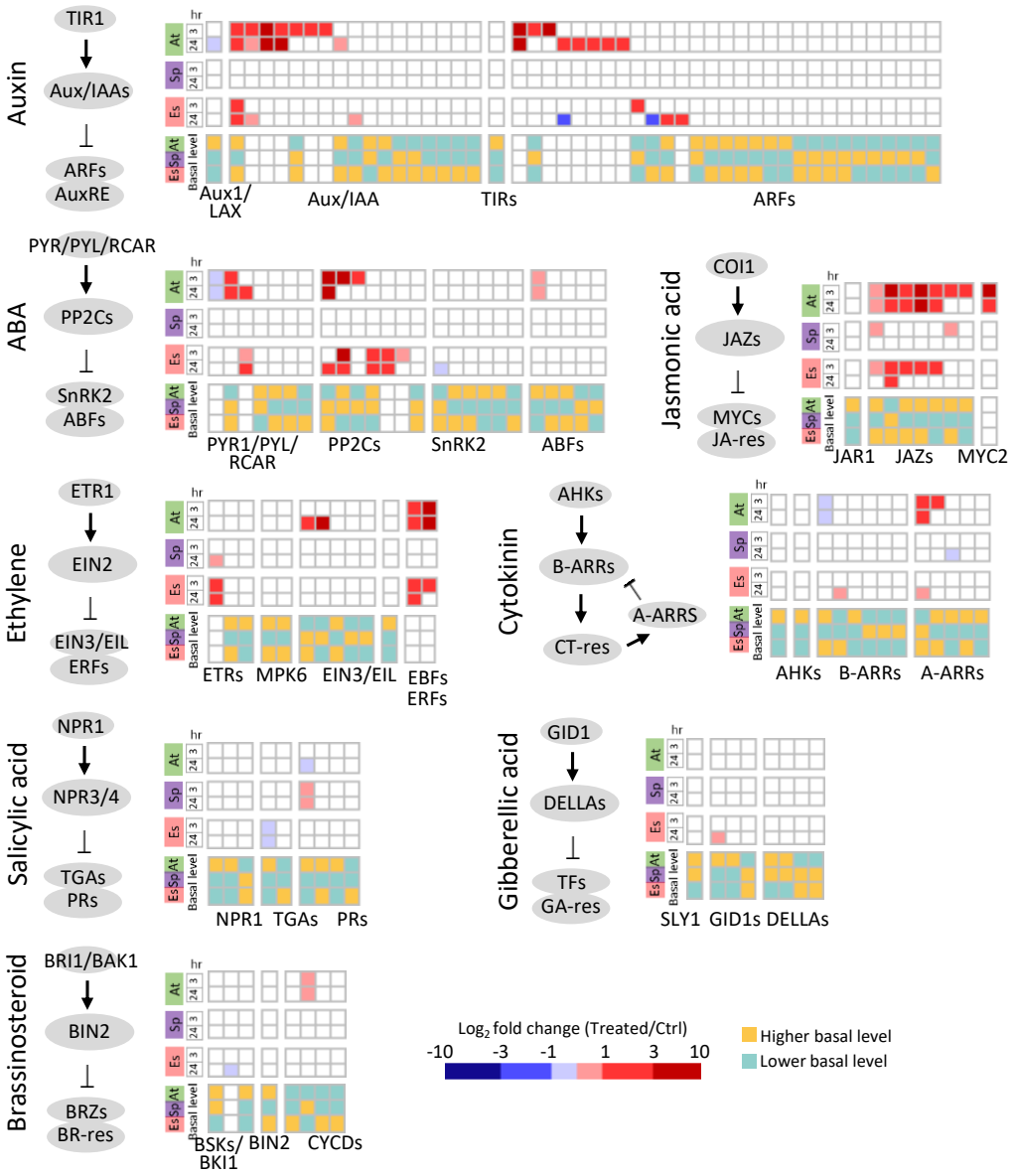

Figure S6: Hormonal signaling pathways in response to salt treatment in *Arabidopsis thaliana, Schrenkiella parvula,* and *Eutrema salsugineum*. Expression responses of genes associated with hormonal signaling pathways obtained from KEGGs. Note that only genes that were significantly different at either basal level condition or under salt treatments were shown. Orthologs in the three species are indicated as high (yellow), low (blue), and indistinguishable levels between species (no-color) assigned to relative basal expression levels

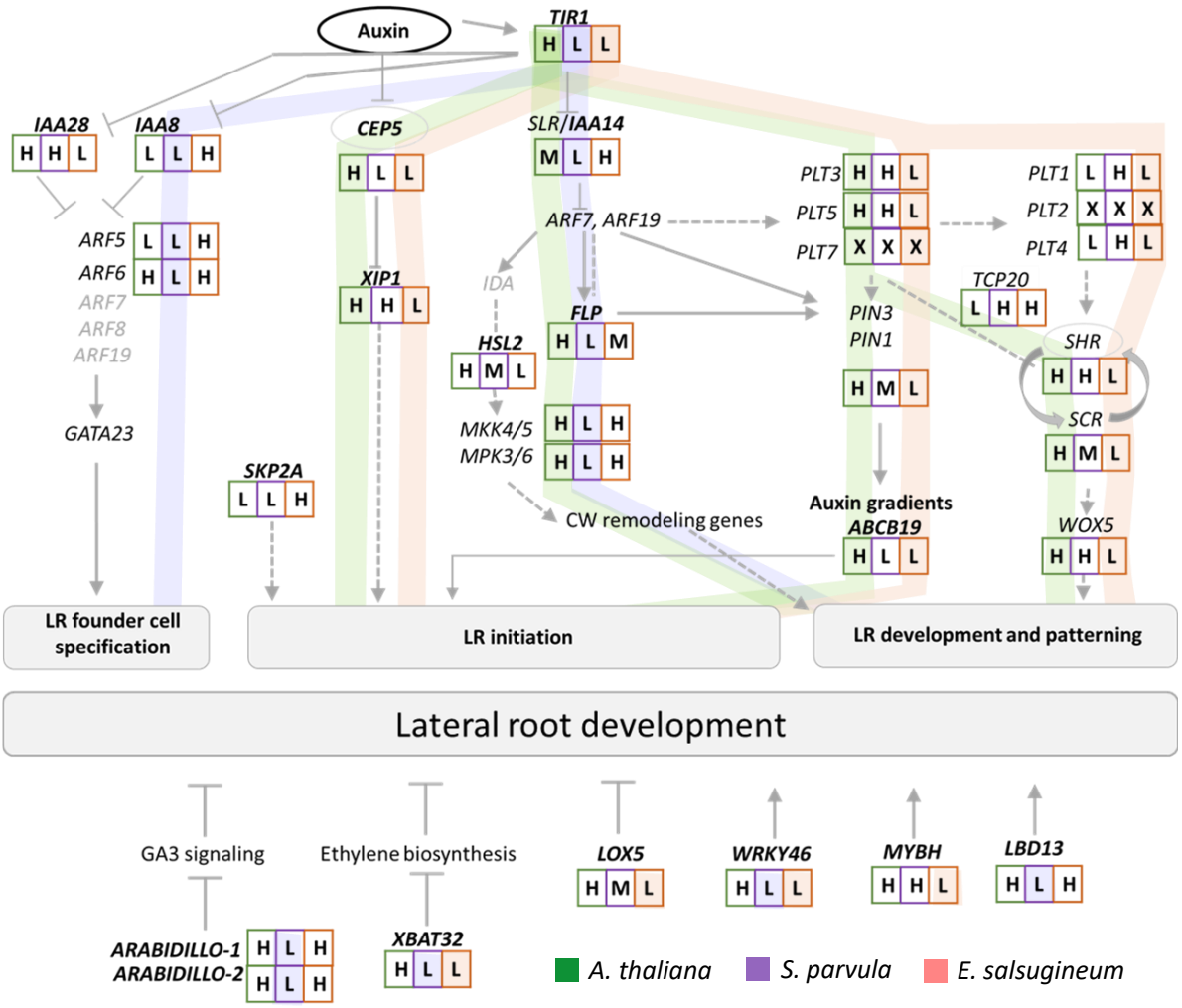

Figure S7: Lateral root development gene network adopted from Banda et al., 2019 and Rybel et al., 2010. The expression levels of orthologs were annotated as high (H), medium (M), or low (L) relative to each other at basal levels in each ortholog group. Specific paths in the network in which *S. parvula* and *E. salsugineum* consistently regulated to inhibit lateral root formation were highlighted in ribbons across the network in species-specific colors.

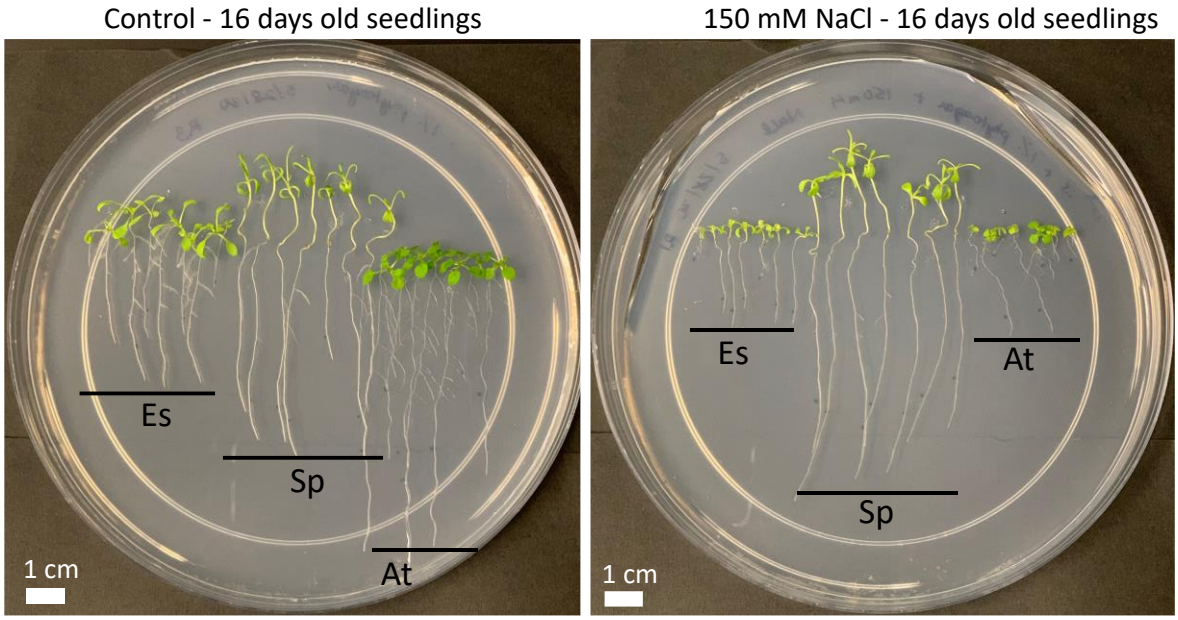

Figure S8: Root growth of *E. salsugineum*, *S. parvula* and *A. thaliana* before and after salt treatments. *S. parvula* (Sp) promoted primary root growth and reduced lateral root formation while *E. salsugineum* (Es) showed slower primary root growth with reduced lateral root number compared to *A. thaliana* (At) roots that showed severe root growth inhibition under salt stress. Five-day-old seedlings were treated for 11 days on plates supplemented with 150 mM NaCl.

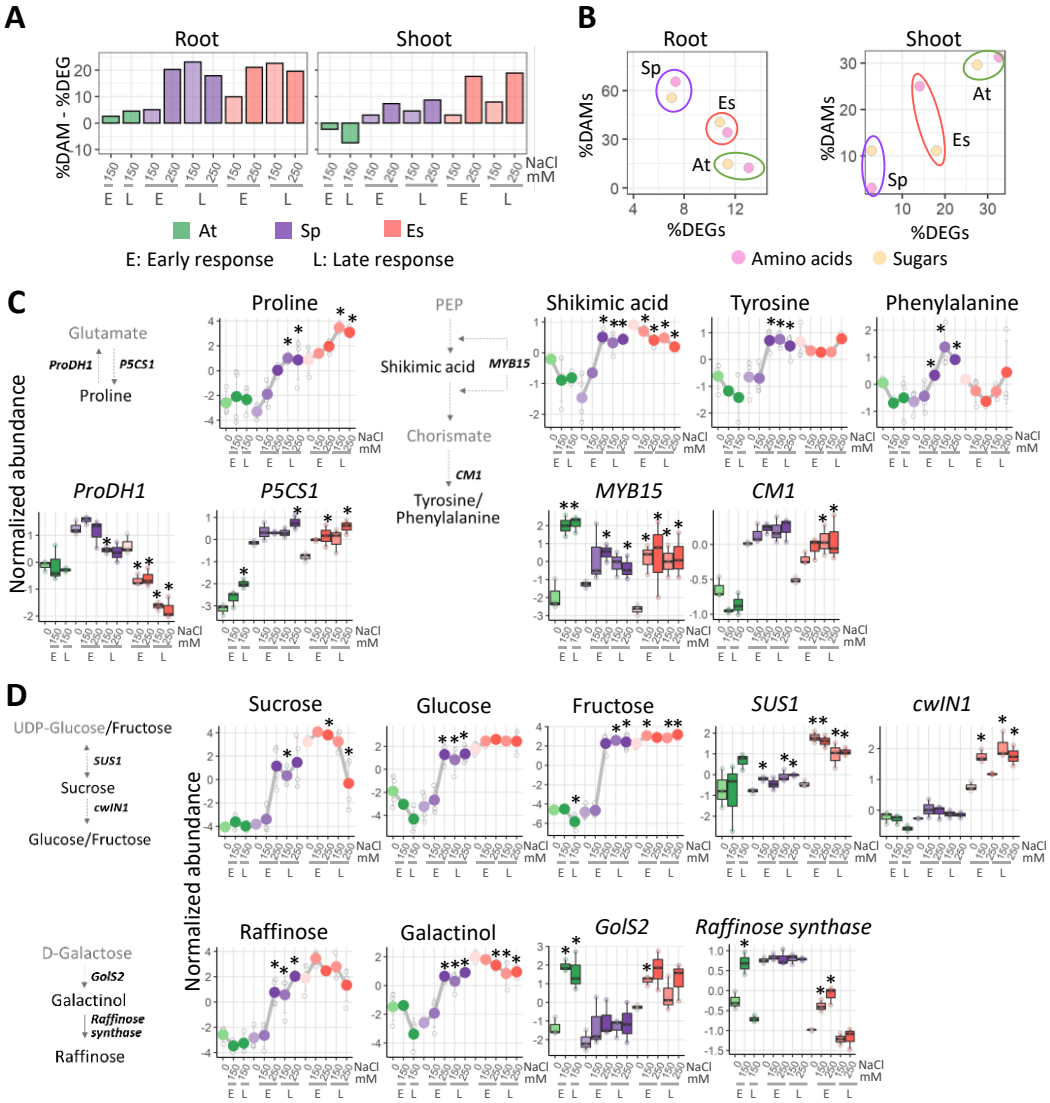

Figure 5: Coordination between differently expressed genes and differently abundant metabolites during responses to salt in *Arabidopsis thaliana, Schrenkiella parvula,* and *Eutrema salsugineum*. [A] The difference in percent change in total differentially expressed genes (DEGs) and total differently abundant metabolites (DAMs) in response to salt treatments. [B] % DEGs and % DAMs involved in the metabolism of amino acids, sugars, and their immediate derivatives (GO:0006520 and GO:0005975). [C and D] Selected pathways in amino acids and sugar metabolism. Line graphs represent normalized Log2 relative metabolite abundance. Boxplots represent normalized expression values. Center line shows median; box indicates interquartile range (IQR); notch is for 1.58 × IQR/sqrt(n); whiskers show 1.5 × IQR. Asterisks indicate DEGs and DAMs assigned using 3-4 biological replicates. Early (E) and late (L) responses for transcripts refer to 3 and 24 hr. E and L responses for metabolites refer to 24 and 72 hr. Metabolites are shown in the backbone of the pathway while genes encoding for key enzymes/transcription factors are placed beside arrows. Black labels in pathway maps indicate quantified metabolites and genes while grey labels indicate metabolites not quantified.

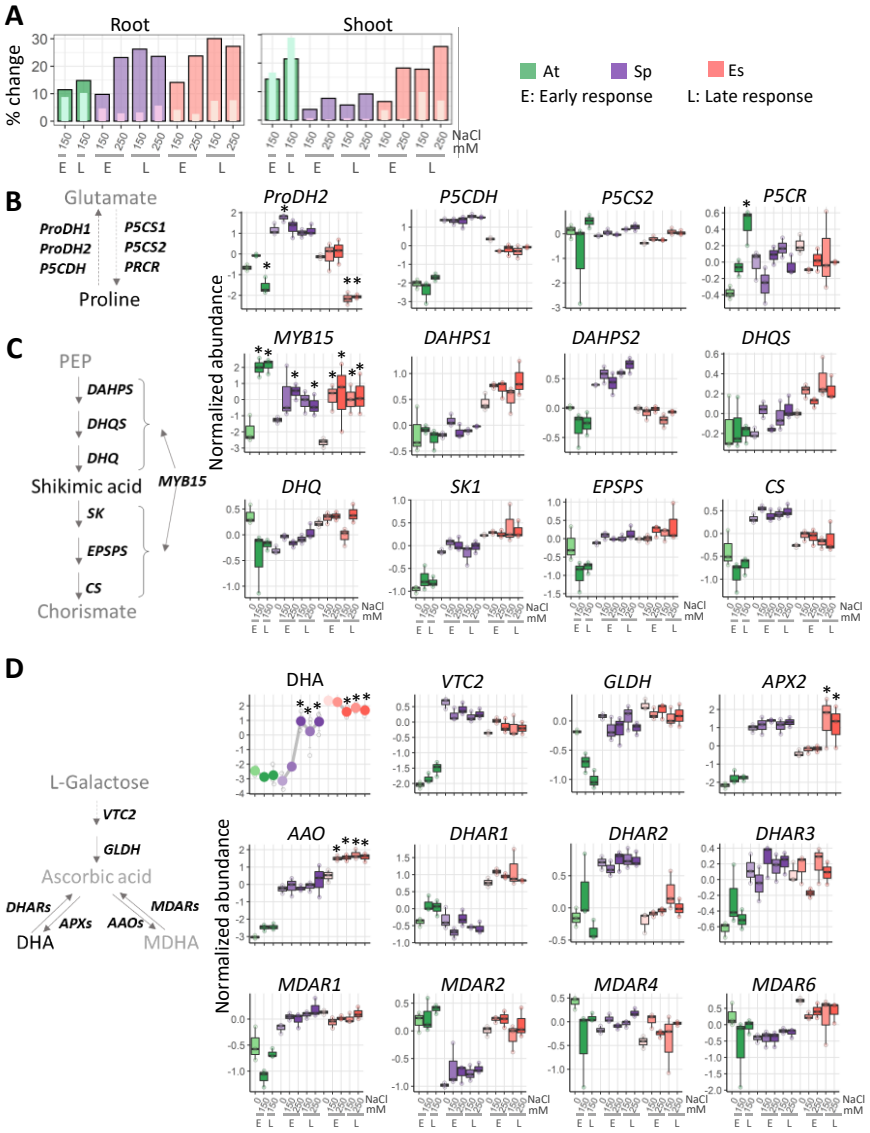

Figure S9: Metabolite abundance and expression of associated genes encoding the enzymes in shikimic acid and ascorbic acid pathways. [A] percent change in total differentially expressed genes (DEGs) and total differently abundant metabolites (DAMs) in response to salt treatments. [B] pathway involved in proline metabolism. [C] pathway involved in the conversion from phosphoenolpyruvate to chorismate. [D] pathway involved in ascorbic acid metabolism. Line graphs represent normalized Log2 relative metabolite abundance. Boxplots represent normalized expression values. Center line shows median; box indicates interquartile range (IQR); notch is for 1.58 × IQR/sqrt(n); whiskers show 1.5 × IQR. Asterisks indicate DEGs (Differently expressed genes) and DAMs (Differently abundant metabolites). Early (E) and late (L) responses for transcripts refer to 3 and 24 hr. E and L responses for metabolites refer to 24 and 72 hr. Metabolites are shown in the backbone of the pathway while genes encoding for key enzymes/transcription factors are placed beside arrows. Black labels in pathway maps indicate quantified metabolites and genes while grey labels indicate metabolites not shown.

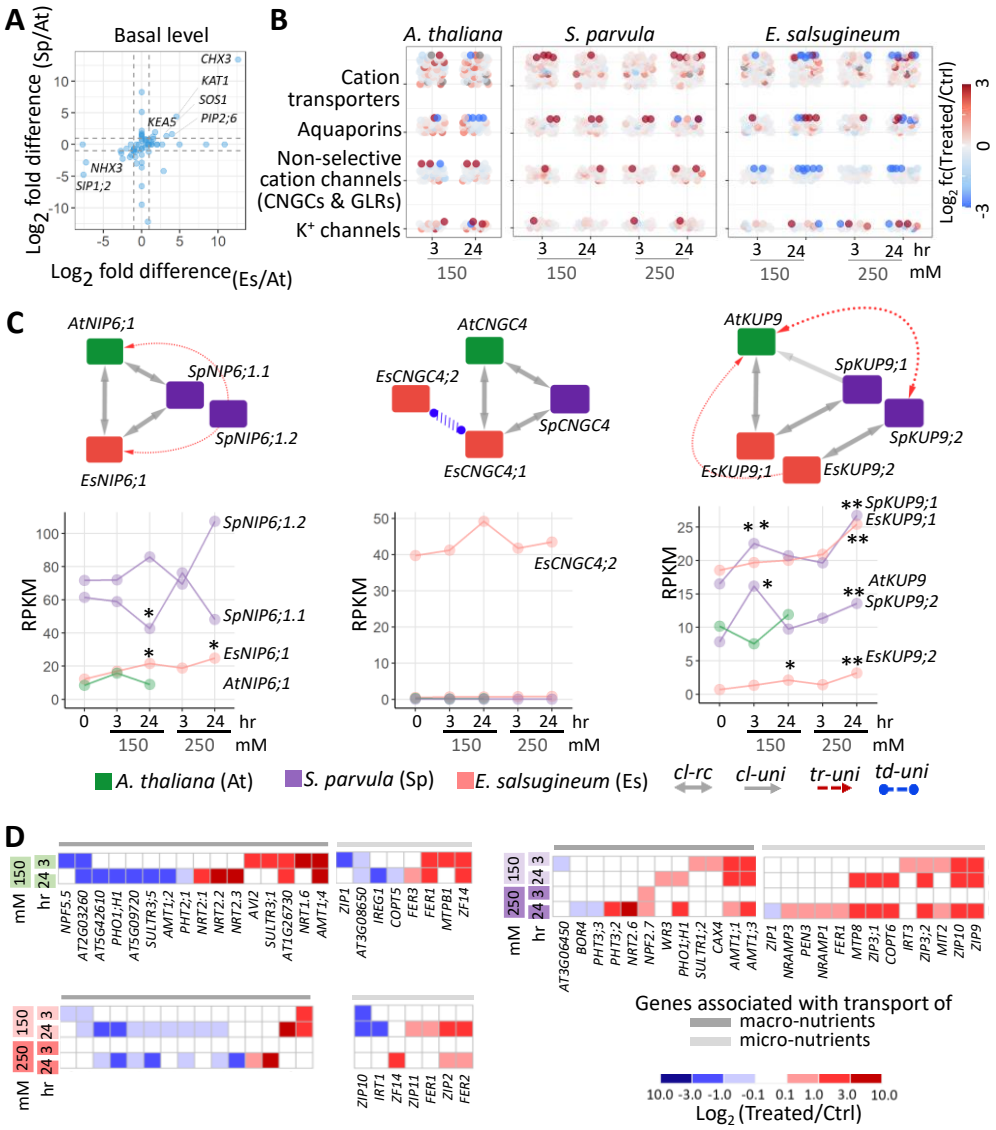

Figure 6: Basal and differential expression associated with salt and nutrient transport in *Arabidopsis thaliana, Schrenkiella parvula,* and *Eutrema salsugineum*. [A] Basal level expression given as fold changes between species. The dashed lines indicate 2-fold differences to highlight genes either highly suppressed or highly expressed in the extremophytes in roots at control conditions. [B] Aggregated expression profiles of transporters/channels associated with Na^+/K^+ transport activity during salt treatments. [C] Selected cation transporters that showed higher gene copy number in extremophytes in ortholog groups and their expression during salt treatments. Nodes of each ortholog network is assigned with species colors connected by edges based on the relationship properties of the homologs. Edges show relationships for co-linear reciprocal orthologs (cl-rc), co-linear unidirectional orthologs (cl-uni), transposed -unidirectional duplicates (tr-uni), or tandem duplicated-unidirectional paralogs (td-uni). Asterisks indicate differentially expressed genes identified at *p-adj ≤ 0.05 and ** p-adj ≤ 0.01. N= 3 (at least 4 plants per replicate). [D] Genes associated with nutrient transport identified in Figure 3C.

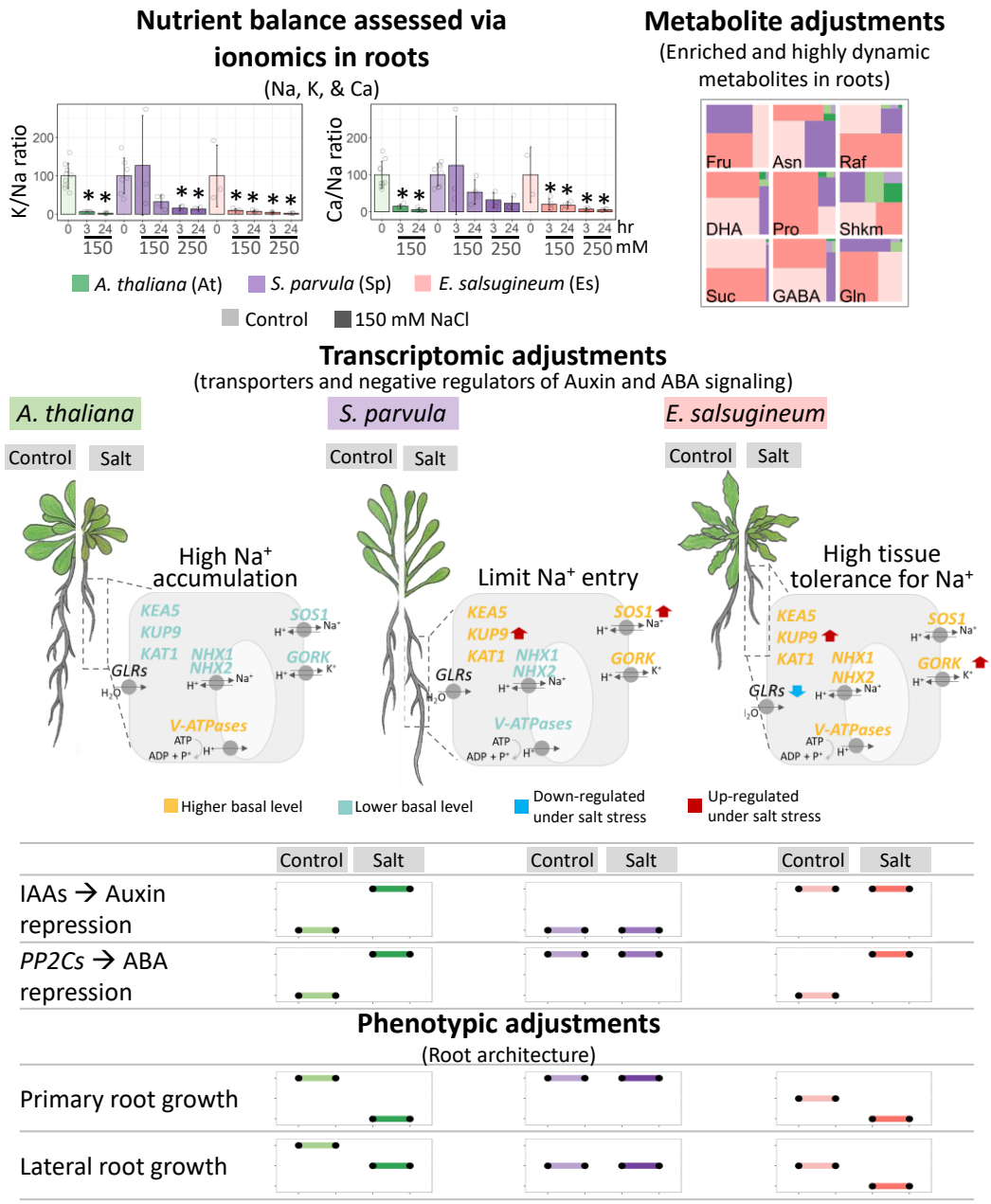

Figure 7: Summary of ionomic, metabolomic, transcriptomic, and phenotypic adjustments and preadaptation trends to salt stress in *Arabidopsis thaliana*, *Schrenkiella parvula* and *Eutrema salsugineum* roots. Top 9 metabolites that increased abundance in *S. parvula* were Fru, fructose; Asn, asparagine, Raf, raffinose, DHA, dehydroascorbic acid; Pro, proline; Shkm, shikimic acid; Suc, sucrose, GABA, gamma-aminobutyric acid; Gln, glutamine. Orthologs in the three species are indicated as high (yellow), low (blue) assigned to relative basal expression levels. Blue and red indicate the induction and suppression gene expression, respectively. KEA5, K^+ efflux antiporter 5; KUP9, K^+ uptake permease 9; KAT1, K^+ channel in *Arabidopsis thaliana* 1; GLRs, glutamate-like receptors; NHX1/2, Na^+/H^+ exchanger1/2; V-ATPases, vacuoles-ATPases; SOS1, salt overly sensitive 1; GORK, gated outwardly-rectifying K^+ channel.